UNIVERSITY OF CALIFORNIA,
IRVINE

Spreading and Leidenfrost in Superfluid Helium

DISSERTATION

Submitted in partial satisfaction of the requirements of

DOCTOR OF PHILOSOPHY

in Physics

by

Matthew L. Wallace

Dissertation Committee:
Professor Peter Taborek, Chair
Professor Zuzanna Siwy
Assistant Professor Albert Siryaporn

DEDICATION

This work is dedicated to the all those who love
curiosity and the spirit of science.

Contents

1 List of Figures

2 Acknowledgments

I would like to acknowledge the King Abdullah University of Science and Technology (KAUST) for funding this research under Grant No. URF/1/2621-01-01. I'd also like to acknowledge my advisor, Professor Peter Taborek, and a few other professors I've worked with, Professors Sigurdur Thoroddsen and Professor Zuzana Siwy. I would also like to acknowledge my colleagues Michael Milgie, David Mallin, Jeffrey Botimer, and Ken Langley. I'd also like to acknowledge the support of my family, without which this all would not have been possible.

3 Vita

Education

University of California, Irvine — June 2020
Ph. D. in Physics
Thesis Title: "Spreading and Leidenfrost in Liquid Helium Drops"
Thesis Advisor: Peter Taborek

University of California, Irvine — June 2018
M. S. in Physics

University of Utah — May 2014
B. S. in Physics

Skills

Laboratory: Low-temperature physics, cryostat operation, high-speed imaging, experimental equipment design and fabrication, high-vacuum technology, machine shop
Software: Mathematica, Inventor (CAD), Python, IDL, LabVIEW, COMSOL, Microsoft Office

Research Experience

Graduate Student Researcher, University of California, Irvine — 2016-Present

Advisor: Peter Taborek
Low-temperature physics, superfluids and superconductors, experimental design, high-speed imaging

Cosmic Ray Research Assistant, University of Utah — 2014
Advisor: John Belz
Create data analysis software, maintain experimental equipment

Astronomy Research Assistant, University of Utah — 2013-2014
Advisor: Anil Seth
Researching Star Clusters with Citizen Science Data

Astronomy Imaging Specialist, University of Utah — 2012
Advisor: Shane Larson
Image celestial objects with a 20" telescope

NASA Intern, NASA Langley Research Center — 2011
Advisor: K. Chauncey Wu
Calculate non-optimum factors based on the Space Shuttle

Microgravity Researcher — 2011
Advisor: Jan Sojka
Research heat transfer in a microgravity aircraft

Teaching Experience

Teaching Assistant, University of California, Irvine — 2014-2015

Teaching assistant for standard undergraduate physics courses

Teaching Assistant, University of Utah — 2012
Teaching assistant for observational astronomy class

Publications

Impact and Lifecycle of Superfluid Helium Drops on a Solid Surface
M. Wallace, D. Mallin, M. Milgie, K. Langley, A. Aguirre-Pablo, S. Thoroddsen, P. Taborek
Submitted to Physical Review Fluids

Observation of the Origin of Downward Terrestrial Gamma-Ray Flashes
J.W. Belz, [134 authors], **M. Wallace**, [11 authors]
Submitted to Journal of Geophysical Research: Atmospheres

The Leidenfrost Effect in Liquid Helium
M. Wallace, D. Mallin, M. Milgie, K. Langley, A. Aguirre-Pablo, S. Thoroddsen, P. Taborek
In preparation

A Hybrid Resistive Pulse-Optical Detection Platform for Microfluidic Experiments
P. Hinckle, [3 authors], **M. Wallace**, [3 authors] Scientific Reports 7, Article number: 10173 (2017)

PHAT Stellar Cluster Survey. II. Andromeda Project Cluster Catalog
L. Johnson, [2 authors], **M. Wallace**, [8 authors], 2015, Astrophysical Journal, 802, 127

Hardware-based Non-Optimum Factors for Launch Vehicle Structural Design
K. Wu, J. Cicero, and **M. Wallace**, 2014, SAWE International Journal of Weight Engineering, Volume 74, No. 2

Selected Talks

Impact of Superfluid Drops 2019
APS Department of Fluid Dynamics, Seattle, WA

Leidenfrost-like Non-Coalescence of Liquid Helium Drops 2018
APS Department of Fluid Dynamics, Atlanta, GA

Spreading of Normal and Superfluid Helium Drops 2018
APS March Meeting, Los Angeles, CA

Impact, Spreading, and Splashing of Superfluid Drops 2017
Droplets 2017 Conference, Los Angeles, CA

Citizen Science with the Andromeda Project 2013
University of Utah Research Symposium, Salt Lake City, UT

Development of Structural Non-Optimum Factors for Launch Vehicle Design 2011
NASA Langley Research Center, Hampton, VA

Grants and Awards

Undergraduate Research Scholar Designation 2014
University of Utah

Undergraduate Research Opportunities Program 2013
For work on The Andromeda Project

Microgravity Research Fellowship 2011
Utah State University
For microgravity research

Groups

Undergraduate Students Supervised: Tejas Dethe (2018-2019),
Alisa Snow (2019), Nicholas Jaber (2019), Jonathan Fung (2019)

4 Abstract of the Dissertation

Spreading and Leidenfrost in Liquid Helium Drops

Matthew L. Wallace

Doctor of Philosophy in Physics

Professor Peter Taborek, Committee Chair

We have used high-speed video and interferometry to investigate the impact, spreading, and eventual contraction of superfluid ^{4}He drops on a sapphire substrate in a saturated atmosphere of helium vapor. We find the counter-intuitive result that the short-term kinetic spreading of superfluid drops (time $t < 10$ ms) is qualitatively similar to both normal helium and to conventional fluids at room temperature. In contrast, the contraction phase of the superfluid drops is highly unusual. Superfluid drops survive for only a few seconds on the substrate due to superflow out of the drop into the surrounding helium film. The drop lifetime is strongly dependent on temperature and diverges at the superfluid transition temperature $T_\lambda \sim 2.17K$. The retracting drops undergo a geometry-dependent two-phase contraction, which includes a toroidal phase where the radius decreases linearly in time, and subsequently a spherical cap phase where the radius decreases with the square root of time. The receding contact angle is temperature dependent and becomes small near T_λ. We also observe that the superfluid outflow causes surprising edge effects, including the emergence of satellite droplets on the perimeter of the expanding drop, as well as ragged and frayed drop edges at lower temperatures. Additionally, we present the results of our investigation of the Leidenfrost effect in liquid helium droplets impacting on a solid surface in an optical cryostat at temperatures between 3.5 K and 5.2 K at saturated vapor pressure. We use high-speed video to image the impacting drops and record the minimum temperature difference ΔT necessary to levitate the drops, and also to observe the lifetime, changing radius, and termination of levitation. We observe that the Leidenfrost onset temperature T_L is a function of the ambient

temperature and runs approximately parallel to the vapor pressure curve, with a lower ΔT needed to levitate the drop at higher temperatures. We also observe that the ΔT needed to levitate the drops is much smaller than has been predicted by previous authors examining film boiling in helium, requiring only 1-70 mK for levitation. We compare our results to previous models for T_L, and we calculate the a vapor film thickness of $\sim$ 2-6 μm, much thinner than for experiments for water at room temperature. We show that this levitation cannot be attributed to film squeeze-out or to the Marangoni effect, and we observe that helium drops levitate over both a warmer solid surface and a warmer thin layer of liquid helium.

5 History, Background, and Motivation

The study of drop impact and drop levitation has a rich and varied history. From the initial observations of levitating drops by Johann Gottlob Leidenfrost to research studying the effects of droplet jets in rocket motors, liquid drop phenomena have worked quietly, and almost anonymously, to shape our modern world. It was in light of the importance of drop impacts - and our curiosity about the hydrodynamics of normal fluid and superfluid helium - that we decided to do an experiment to study the difference between the impact behavior of normal fluid helium drops and superfluid helium drops. For this experiment, we completed the construction of a new cryostat in collaboration with the Thoroddsen group at the King Abdullah University of Science and Technology (KAUST); this new cryostat had a base temperature of 1.2 K and 25 mW of cooling power. The idea for the experiment was simple - we'd drop normal fluid heluim droplets and superfluid helium droplets on a solid surface, film them with a high-speed camera, and observe how drop impacts in the two fluid states behaved differently. As simple as it might seem, there are substantial differences between these two fluid states that suggested that the impact behavior might be quite different. First, normal fluid helium has a finite viscosity, while superfluid helium has zero viscosity. This zero-viscosity property of superfluid helium raises some interesting questions - will the drop spread infinitely fast? Will it fully wet the surface? With no resistance to fluid flow, what will and impacting drop do? Additionally, superfluid helium can contain quantum vortices, and we were interested in finding out if the formation of these quantum vortices would have any effect on the impact and spreading.

The short answer to the difference between normal fluid helium drop impacts and superfluid drop impacts is this: in the first 20 ms, not much; but after that, the behavior of the two fluid states is completely different. Normal fluid helium spreads out like conventional (room temperature in air) fluids, but with a slightly different exponent ($\sim 1/7$) than is usually observed for such fluids. By contrast, superfluid drops quickly contract and disappear in seconds as the entire volume of the drop drains through the thin adsorbed

layer of helium that is stuck to the impact surface. This is the long and the short of it, and the rest of our analysis of these drop impacts is our attempt to quantify these differences. Though we had anticipated some differences between the impact behavior of the normal fluid and superfluid, we discovered the Leidenfrost effect in liquid helium quite by accident. The Leidenfrost effect is where a drop levitates above a heated surface on a cushion of its own vapor, as when a drop of water levitates over the surface of a hot frying pan on a kitchen stove. This effect has been described extensively in scientific literature, but many mysteries still remain. For most liquids, the temperature of the hot surface must be quite high to induce levitation in a liquid droplet; indeed, for water on a hot frying pan, the frying pan surface must be about 115 K hotter than the boiling temperature of water for the drop to levitate. To our knowledge, the effect has not previously been observed in liquid helium. As part of our experimental setup, we had glued s small ohmic heater to the side of the sapphire impact surface so we could clear the impact surface of visible puddles of liquid helium before dropping drops onto the surface. By turning up the voltage input to this ohmic heater, we saw that we could get the drops to levitate. We also noticed that the drops levitated on their own above a temperature of about 4.2 K with no heat input from the ohmic heater. Initially we thought the effect was a novelty, something that was fun to look at but not very scientifically interesting. Our further investigations have revealed an observation of the smallest temperature difference ΔT ever recorded to initiate Leidenfrost levitation. We hope that these results will shake up the Leidenfrost world, if only a little. Another unexpected surprise was the appearance of thin-film interference fringes on the drops as they sat on the impact surface. This effect was very robust, and not only did we have no trouble duplicating the effect, we couldn't get rid of the fringes if we tried, at least in the side view. These fringes provided excellent data of drop topography and allowed us to measure the drop height, shape, and contact angle with ease. Again, I'd like to say that we'd planned all along to use this thin-film interference technique, but it was another gift from the natural world.

I present this dissertation to you. It represents the collective efforts of a small group of scientists working in our own corner of the galaxy, struggling to understand the mysteries of the cosmos while trying to create a place in that cosmos for us to exist and thrive. It is my hope that in a hundred generations, the torch of science will burn as a candle in the darkness for all those who love curiosity and the spirit of knowledge.

6 Introduction: Superfluid Spreading

Liquid drop impact and spreading are ubiquitous phenomena with diverse applications. They have been investigated using classical fluids under a wide variety of conditions, including drop impact on a solid dry surface [4, 5, 6, 7, 8, 9], on a thin liquid film [10, 11, 12], in an atmosphere of ordinary air, and in atmosphere of air mixed with the fluid's own vapor [13]. Most of these studies have focused on either short-term (inertia-driven) spreading driven by the kinetic energy of impact, or long-term spreading, driven by either surface tension or gravity. The experiments typically record the height h (or thickness) of the impacting/spreading drop and the radius of the drop footprint r as it spreads as a function of time t. For the short time regime of kinetic impact, the drop radius as function of time scales as $r(t) \sim t^a$ with $a = 1/2$ for nearly all fluids regardless of wettability due to the balance between interfacial tension and inertia [14, 15]. For non-volatile fluids that completely wet a substrate, a spreading drop will eventually evolve into a pancake shape with a large radius and a microscopic thickness[16]. The approach to this state can be described by power laws $r(t) \sim t^\alpha$, with the exponent α being determined by a balance between the driving forces and dissipation in the drop. For surface tension driven spreading of spherical cap drops, $\alpha = 1/10$, which is known as Tanner's law. Other geometries and driving forces yield values of α in the range $0.1 - 0.15$ [6, 17, 18]. In the hydrodynamic lubrication approximation limit, the prefactor for the power law is inversely proportional to the fluid's dynamic viscosity η; for the case of gravity driven spreading[17], the drop radius is given by

$$r(t) \sim V^{3/8}\left(\frac{\rho g t}{\eta}\right)^{1/8}, \tag{1}$$

where ρ is the fluid density, V is the drop volume and g is the acceleration due to gravity. Equation 1 shows that in a classical fluid, the dynamics of spreading are related to viscous dissipation. Superfluids can flow without any dissipation, and even if there is dissipation,

the mechanism involves nucleation and generation of vorticity [19] which is quite different from conventional viscous dissipation. For these reasons, theorists have suggested [20, 16] that superfluid spreading kinetics might be distinctly different from the classical case. Another assumption that underlies asymptotic predictions such as Eq. 1 is that the fluid completely wets the substrate and that the equilibrium contact angle is zero. Liquid ^{4}He in both the normal and superfluid states is thought to completely wet all substrates except cesium[21, 22, 23, 24]. There nevertheless are intriguing experimental results which show a finite contact angle in the superfluid state[25, 26, 27] on conventional substrates. These observations of a static superfluid meniscus with a finite contact angle are presumably due to thermal inhomogeneities or pinned vorticity.

Our experiment monitors the dynamic contact line of a superfluid drop impinging with an initial velocity of approximately 0.4 m/s onto a sapphire substrate covered by an equilibrium thin adsorbed film of superfluid (de Gennes' "moist" case[16]). Despite the extremely low viscosity, the initial inertia-driven phase of spreading of the superfluid is remarkably similar to the case of classical fluids, and the kinetic energy of impact is essentially dissipated within 20 msec, resulting in a pancake shaped drop with a footprint radius roughly 5 times the radius of the initial drop. Rather than continuing to spread like a classical fluid, the superfluid drop contracts with a finite receding contact angle and disappears within a few seconds. The dynamics are qualitatively consistent with a model developed by Herminghaus[28, 27] which balances the Bernoulli pressure of a superflow at the critical velocity from the drop into the surrounding film against the Laplace pressure due to the curvature of the drop and the pressure due to van der Waals forces.

The experimental cell shown in Figure 1 was contained inside an optical cryostat consisting of a vacuum vessel and two concentric gold plated copper heat shields held at a temperature of 40 K and 4 K respectively, using a closed cycle refrigerator, also used in a recent related study on jet breakup[29]. The windows in the shields which provided optical access were constructed using a sandwich structure of KG1 glass (to absorb IR radiation)

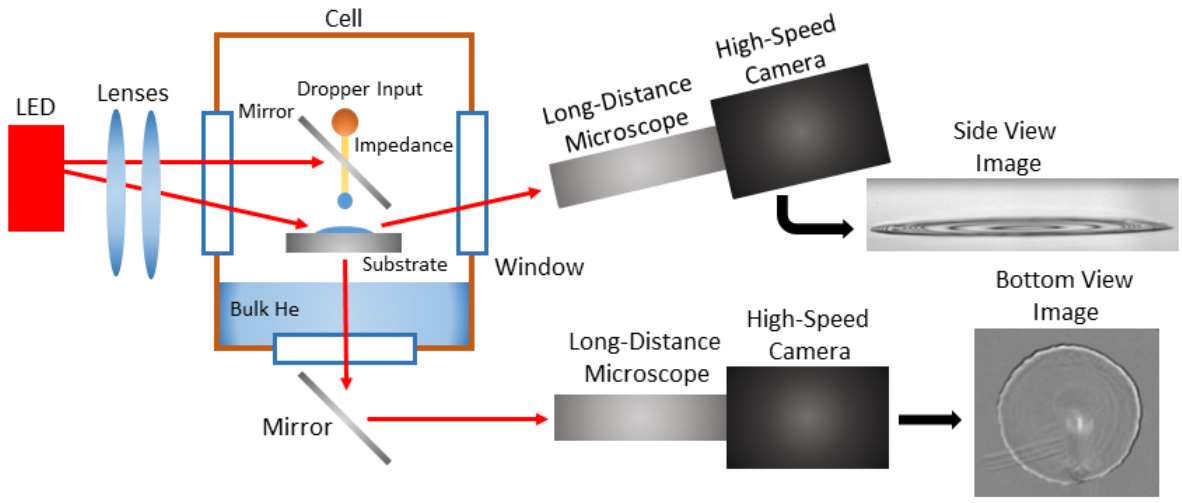

Figure 1: Schematic diagram of the experimental cell and imaging setup. The cell was mounted inside a cryostat capable of reaching and maintaining temperatures of 1.2 K - 5.2 K. The gravity-fed dropper released the drops onto the sapphire impact surface. An LED and collimating lenses were used to illuminate the drops and impact surface. Two camera positions were used, one for side viewing and one for bottom viewing. A mirror was used for the bottom viewing, and a hole was drilled in the center of the top mirror allowing the nanopipe dropper nozzle to pass through.

and sapphire (to provide a thermal link to the shield). The cell itself was equipped with a separately pumped ^{4}He pot which could maintain the temperature between 1.2 K and 5.2 K. The helium drops were formed by applying a small over-pressure of 2-50 Torr above the saturated vapor pressure to a flow impedance nozzle made from a glass capillary with an inner diameter of 10 μm and an outer diameter of 365 μm. By adjusting the over-pressure, drops with a radius of 0.5 mm would fall from the dropper at predictable intervals of approximately 30 seconds.

The drops fall 1 cm and impact onto a cylindrical piece of sapphire 31.7 mm in diameter and 19 mm thick. A small ohmic heater with superconducting leads was glued onto the side of the sapphire to provide heat for clearing the surface of extant liquid helium; the system was allowed to return to equilibrium before measurements were taken. An LED light of wavelength 632 nm was used to illuminate the impact surface. The illumination system and the high-speed camera used for imaging from the side was mounted at a downward angle of 6.4 degrees. A fill line, separate from the dropper line, was used to add

or remove helium from the cell; during operation, there was always a reservoir of bulk liquid at the bottom of the cell. For the bottom view imaging, an aluminum mirror was used to reflect the light, and an angled hole was drilled in the center of the mirror to allow the capillary nozzle to pass through.

To collect data, the dropper line was pressurized as describe above, and the high-speed camera was used to take video of the impacting drops at 100-25,000 frames per second (fps). The individual frames were then extracted from the video and the drop radii measured. In a saturated helium vapor environment, even a nominally 'dry' surface is covered with a microscopically thin layer of helium which is stabilized by van der Waals forces. A quartz crystal microbalance (QCM) was occasionally used in place of the sapphire substrate to measure the thickness of this film, but was not used for drop impact and lifecycle measurements. The QCM showed that the equilibrium helium film thickness, presumably limited by the gravitational potential difference between the substrate and the bulk liquid reservoir at the bottom of the cell, was in the range of 20-40 nm thick. The drops were highly mobile on this adsorbed film, and it was important to precisely level the cryostat to prevent the drops from drifting off the edge of the substrate.

Side view images of drops show dark and light fringes due to interference between the liquid-vapor interface at the top of the drop and the liquid-sapphire interface at the bottom of the drop. The change in liquid film thickness per fringe (light to light or dark to dark) is

$$\delta h = \frac{\lambda}{2\sqrt{n_{film}^2 - \sin^2\theta_{inc}}}, \tag{2}$$

with light wavelength λ, helium film index of refraction $n_{film} = 1.03$, and incident angle θ_{inc} . Interference lines were only visible in the side view; in the bottom view, the low index of refraction of liquid helium and the near normal incidence dictates that the reflected waves from the top drop surface are very weak and are not visible to the camera. These interference lines can be used to determine the drop topography and dynamic contact angle, as discussed in the next section. For images taken with a red LED with a

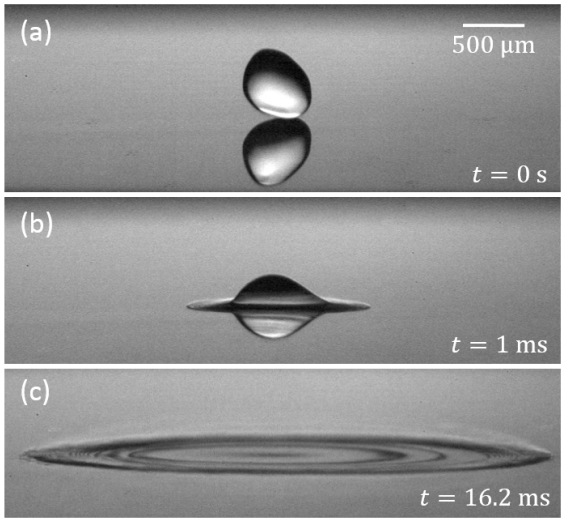

Figure 2: Short-term spreading of a drop at temperature $T = 1.518$ K impacting on the sapphire substrate shown at time t after impact. (a) shows the drop at the moment of impact, and (c) shows the drop near the maximum spreading radius R_{max}. The concentric bands of light and dark are due to interference from regions of different thickness. The image of the drop is reflected in the sapphire surface in (a) and (b). Because of the very low viscous dissipation, initial shape perturbations are not damped out in superfluid drops, so they are often remarkably asymmetric, as in (a).

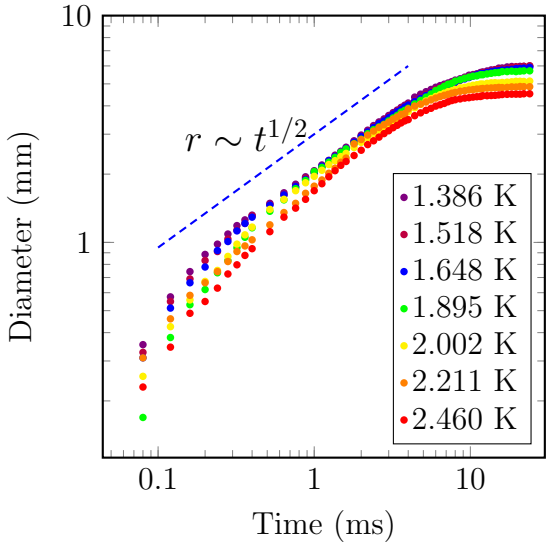

Figure 3: (Color online.) Drop footprint diameter as a function of time after impact at a velocity of $U = 0.45$ m/s for several values of the ambient temperature indicated by colors ranging from violet∼coldest to red∼warmest. The dashed blue line shows a growth rate characterized by an exponent of 1/2 , which is typical of many classical fluids. Although the superfluid fraction varies from zero to 0.93, this does not significantly affect the short term dynamics of spreading. There is a rather abrupt transition to a much slower growth rate near t∼6 ms.

wavelength of 632 nm and illuminated at an angle $\theta_{inc} = 83.6°$ each bright fringe corresponds to a change in film thickness of 1167 nm.

7 Results and Discussion: Superfluid Spreading

7.1 Short-Term (Inertia-Driven) Spreading

The physics of inviscid drop impact is governed by a balance between inertia and surface tension, and is characterized by the Weber number $We = \rho R U^2/\gamma$, where R is the drop radius , U is the imapct velocity, and γ is the liquid-vapor surface tension. The Weber

number in our experiments is ~ 33 for drops impacting at $U = 0.45$ m/s and ~ 145 for drops impacting at $U = 0.94$ m/s (the experimental results of the drops impacting at $U = 0.94$ are shown only in Figure 5; all other data presented in this paper is for drops impacting at 0.45 m/s.) During the first few microseconds after impact, the drop shape can be approximated as a truncated sphere, and the spreading radius of the contact line follows a power law $r \sim t^{1/2}$ for geometric reasons [5, 10]. The subsequent spreading dynamics can be modeled as a shock [8] or using self-similarity[30, 31] at high We or as a singular flow similar to drop coalescence [32, 33] for low We. All of these models predict a power law dependence of the drop footprint radius as a function of time after impact, with an exponent near 1/2; fluid properties affect the prefactor of the power law, but not the exponent. In particular, the inviscid coalescence model predicts

$$r = c\Big(\frac{4\gamma A}{\rho}\Big)^{1/4}\Delta t^{1/2}, \tag{3}$$

for constant c of order unity (determined to be 2-4 in our experiments), initial radius A, and time $\Delta t = t - t_0$ for time t and initial contact time t_0. The inertia-driven spreading of fluids with dynamic viscosities in the range of $10^{-3} - 10^{0}$ Pa·s obey a similar power law with the prefactor c determined by the dynamic viscosity [5, 15, 33]. The inertia-driven shock model of reference [8] also predicts a weak dependence of the prefactor on fluid viscosity. In classical fluids, the inertia-driven regime describes the dynamics until the drop footprint has reached approximately three times the original drop diameter, after which the spreading rate slows down and is described by a power law of the form of Eq. 3. A time Δt_{cross} which characterizes the cross-over from the inertia-driven regime to capillary-viscous spreading regime is[32]

$$\Delta t_{cross} = \frac{R^{13/8}\rho^{5/8}}{\eta^{1/4}\gamma^{3/8}}. \tag{4}$$

The cross-over time has a typical magnitude of a few milliseconds for our impact velocity and temperature range.

The inertia-driven regime in superfluid impact was monitored using high-speed video from both the side view and bottom view. A few frames of a side-view video are shown in Figure 2. Despite the low refractive index, the advancing contact line is clearly visible. A plot of the drop footprint diameter as a function of time for ^{4}He is shown in Figure 3 for temperatures which span the range from above T_λ to $T = 1.38$ K, where the superfluid fraction is 0.93. After ~ 10 ms, the drops transition to a different regime where the contact line essentially stops moving. Using values for normal ^{4}He, Equation 4 gives a value of 3 ms for the cross-over time which is in qualitative agreement with the data. The initial kinetic energy of the drop (approximately 5 nJ) is dissipated within a few milliseconds. In conventional fluids, the dissipation is attributed to complex processes at the moving contact line which are proportional to the viscosity. It is remarkable that a wide variation of the superfluid fraction does not seem to affect the the maximum size or the rate of expansion of the drops.

Another interesting feature of the spreading drops is an instability in the advancing contact line that is associated with superfluidity. In contrast to normal ^{4}He fluid drops, which display smooth edge behavior similar to conventional fluids in air at room temperature, superfluid droplets exhibit spatial structure at the edges that becomes increasingly pronounced at lower temperatures and higher superfluid fractions. In our experiment we used two drop impact velocities corresponding to two drop heights. At the lower impact velocity $U = 0.45$ m/s, the superfluid droplets formed rings of transient satellite droplets around the edges of the spreading drop, shown in a bottom view in Figure 4. These droplets may be a manifestation of the high velocity superflow in the thin film surrounding the drop that we discuss in the next section. At greater impact velocity $U = 0.94$ m/s, in addition to the appearance of satellite droplets, the drop contact line became ragged and frayed, as shown in Figure 5.

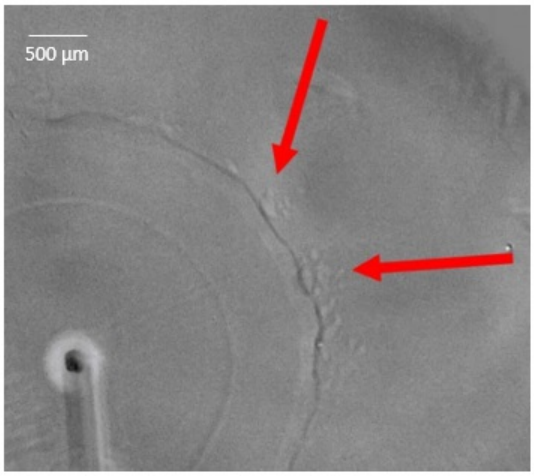

Figure 4: (Color online.) Bottom view of spreading superfluid drop at $T = 1.564$ K, with arrows pointing to the ring of exo-droplets. Most of the drop is in the lower left quadrant; the contact line is clearly visible, and the dark spot in the lower left of the photo is the dropper nozzle.

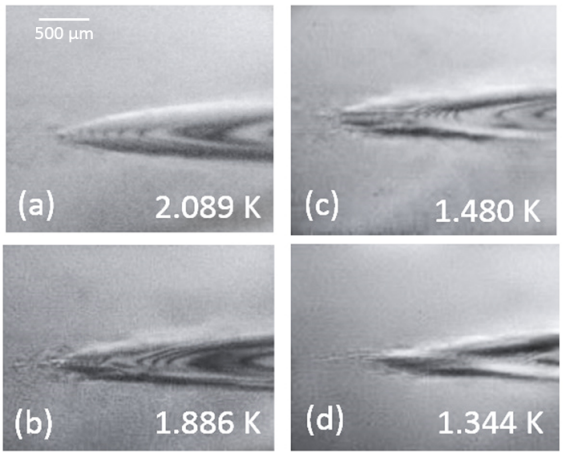

Figure 5: Side view images of the advancing edge of a drop at four temperatures with superfluid fraction varying from 0.28 to 0.95. At an impact velocity of $U = 0.94$ m/s, the edges of the drop become progressively more frayed, ragged, and angular at lower temperatures.

7.2 Droplet Contraction and Lifetime

Although superfluidity has only subtle effects on spreading in the first few milliseconds after impact, it has dramatic effects on the subsequent behavior of the drops. After dissipating the initial kinetic energy, conventional liquids on a wettable substrate will continue to slowly spread, with dynamics described by some version of Equation 1. For volatile drops such as ours, which are surrounded by saturated vapor, the spreading process is eventually truncated by the competing process of evaporation which is driven by the Laplace pressure and the gravitational variation in the vapor pressure in the cell. Above T_λ, helium drops follow this scenario and can be observed to spread for many minutes; the details of this process will be discussed in a subsequent publication. Below T_λ, helium drops begin to contract immediately after the inertia-driven regime and have a lifetime of only a few seconds. Video frames which illustrate the evolution of the drop footprint at $T = 1.6$ K are shown in Figure 6. The lifetime of the drop is less than 2 seconds at low temperature, but rapidly diverges near T_λ, as shown in Figure 7.

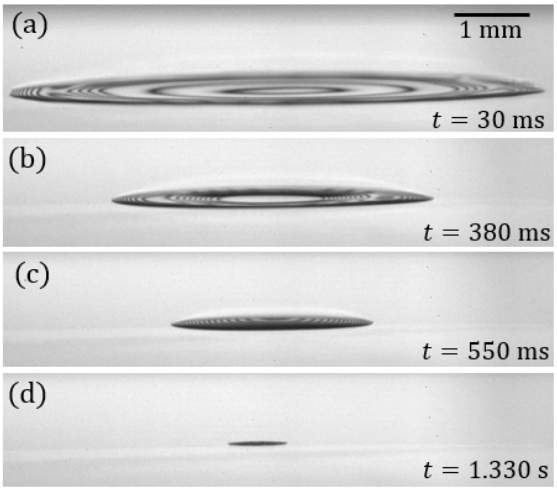

Figure 6: Side view of a ^{4}He drop at temperature $T = 1.626$ K contracting on the sapphire substrate at time t after impact. The concentric bands of light and dark are due to interference from regions of different thickness; the profile of the drop determined from these interference lines is discussed below. The drop disappears after approximately 1.48 seconds.

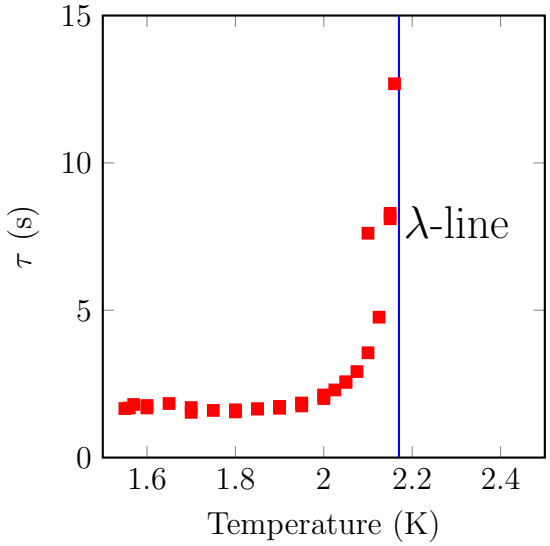

Figure 7: Superfluid drop lifetime τ on the substrate as a function of temperature. The drops last up to 15 minutes above the λ-line.

7.3 Superflow Through the Surface Film

The rapid contraction of the drops cannot be explained by evaporation, which would require pressure differences of the order of 1 Pa or temperature differences of order 10^{-4} K, both of which are difficult to justify in our experimental cell. We checked that injecting 5mW of power into the substrate using the electrical heater had no effect on the drop lifetime. The strong temperature dependence of the drop lifetime near T_λ as well as the much longer lifetimes in the normal state suggest that the mass transfer mechanism out of the drop is superfluid flow. The basic plausibility of this idea is supported by the rough estimate that flow at a critical velocity ~ 1 m/s in the surrounding film of thickness 30 nm can drain the 10^{-7} kg mass of the drop in a few seconds. 1 m/s is well below the Feynman critical velocity $v_F \sim 10$m/s .

A more quantitative understanding of the superflow out of the drop can be obtained by

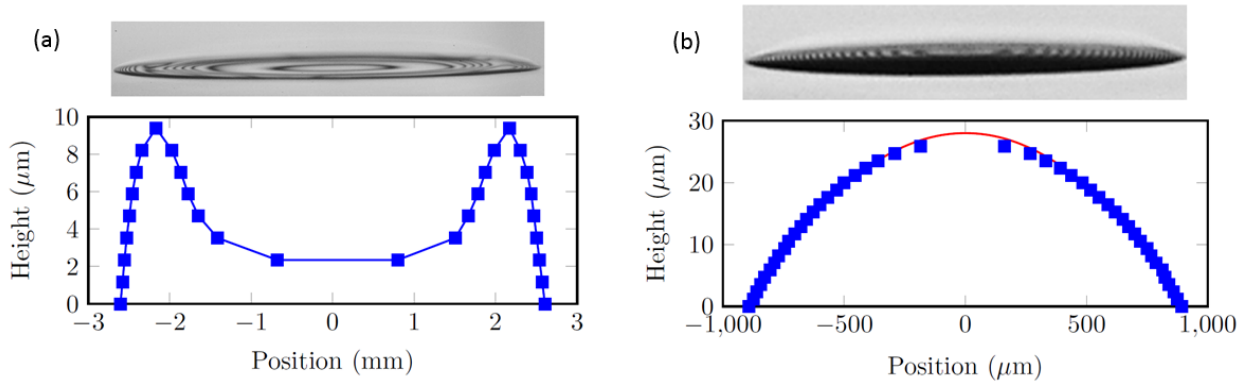

Figure 8: (Color online.) Images of a drop at $T = 1.626$ K with plots of the cross sectional profile computed from interference lines, with each data point in the plots corresponding to a dark fringe in the image. (a) shows the drop during the toroidal phase, and (b) shows the drop during the spherical cap phase. The red line in (b) is a fit to a circle. Note that the horizontal scale in both (a) and (b) is orders of magnitude larger than the vertical scale, so the drops are actually very flat. The drop has lost about 60% of its original volume by the time it reaches the spherical cap phase.

using interferometry to map out the drop topography. The inteference lines are like contour lines on a topographical map, connecting regions of equal height above the impact surface. Using the assumptions that the drop thickness is effectively zero at the nominal contact line, the contrast in the interference image can be integrated to find the drop thickness at any point in the interior. The ambiguity about the sign of the thickness change corresponding to an intensity change can be reconciled by using the fact that the volume of the drop changes slowly on the time scale of a few milliseconds. In particular, we verify that the volume in the initial falling drop shown in Figure 2a is the same as the volume of the drop after the inertia-driven spreading phase shown in Figure 2c.

Figure 8 shows the drop profile constructed in this way for a drop at the beginning of the contraction process. In the toroidal phase shown in Figure 8a, the maximum thickness regions (typical scale $\sim 10\mu$m) of the drop are near the contact line, and the center of the drop is thinner. Figure 8b shows the profile near the end of the drop lifetime, where the drop has evolved into a spherical cap shape with a peak height approximately twice that of the toroidal rim.

More details of the drop profiles as a function of time and temperature are shown in Figure

9. These data show that in the toroidal phase, the receding contact angle is quite constant in time as the drop footprint shrinks. As the drop shrinks, the radius of the central region decreases and it becomes thinner until an instability occurs and the drop makes a rapid and somewhat violent transition to a spherical cap drop, as shown in 8b. This transition between two is also apparent in plots of the drop footprint radius as a function of time, as shown in Figure 12. The plot shows that the radius initially decreases linearly with time, and then makes an abrupt transition to a different regime in which the shrinking rate slows down but then accelerates again near $t = \tau$, the lifetime of the drop. Both of these behaviors are qualitatively consistent with simple geometrical models and the assumption that the superflow is carried by a surface film of constant thickness h moving at a critical velocity v_{crit}. In the initial phase, we approximate the drop as a cylindrical disk of radius $r(t)$ and constant height H,with volume $V(t) = \pi r(t)^2 H$. The rate of change of volume is

$$\frac{dV}{dt} = 2\pi r(t) H \frac{dr}{dt} = -2\pi r(t) h v_{crit}, \tag{5}$$

where the last equality is the flux $j = hv_{crit}$ integrated around the perimeter of the drop. This leads immediately to the conclusion that dr/dt is constant, with

$$\frac{dr}{dt} = -\frac{h}{H} v_{crit}. \tag{6}$$

Using values of $H = 8\,\mu$m, $h = 40$ nm, and $v_{crit} = 60$ cm/s, we see that the radius shrinks at about 3 mm/s, in good agreement with the data in Figure 12. During the second half of the contraction, we empirically observe that the drops contract approximately as

$$r(t) = C_T \sqrt{\tau - t}, \tag{7}$$

with drop radius $r(t)$, time t, constant C_T that depends on the temperature (and thus the superfluid fraction), and total droplet lifetime τ. We again begin with our two assumptions that the fluid again flows out of the drop at v_{crit} and that θ_c remains constant. However, in

the spherical cap phase, the drop will contract differently from the the toroidal phase because of the different geometry. The volume V_{sc} of a spherical cap is given by

$$V_{sc}(t) = \frac{1}{6}h\pi(h_{sc}(t)^2 + 3r(t)^2), \tag{8}$$

with spherical cap height h_{sc}, which is the drop height for spherical cap drops. The slope at the edge of drop (which for small slopes is the contact angle θ_c) is

$$\theta_c = -\frac{r(t)}{\sqrt{R_c(t)^2 - r(t)^2}}, \tag{9}$$

where $R_c(t)$ is the radius of curvature of the drop. If the contact angle remains constant, then $R_c(t)$ must change in time. To find $R_c(t)$, we substitute it into the equation for the contact angle and set the time derivative equal to zero. The result is that $R_c(t)$ must be proportional to $r(t)$ and both $\sim \sqrt{\tau - t}$. Experimentally, we find that $Rc(t)$ decreases with time and is roughly consistent with this prediction, although precise comparison is difficult because of the lack of resolution as the drops become very small.

Understanding the dynamics of the transition from the toroidal phase to the spherical cap phase is a complicated problem that presumably would require a numerical inviscid solver as e.g. ref. [34]. A qualitative understanding of the receding contact angle can, however, be obtained using a simplified 1D model developed by Herminghaus[28] and Poujade et al. [27]. The model is based on several assumptions. First, they assume that the superfluid will respond to a gradient in the chemical potential by generating a flow at a critical velocity which is essentially independent of the magnitude of the gradient. The direction of the flow will be toward lower pressure and/or higher temperature. Assuming a strictly isothermal environment, the chemical potential inside the drop will typically be higher than the bulk fluid in the cell by an amount $\Delta\mu$ (with $\Delta\mu$ representing the difference in chemical potential) due to the higher gravitational potential energy and the increased capillary pressure due to curvature, so we expect a flow out of the drop into the

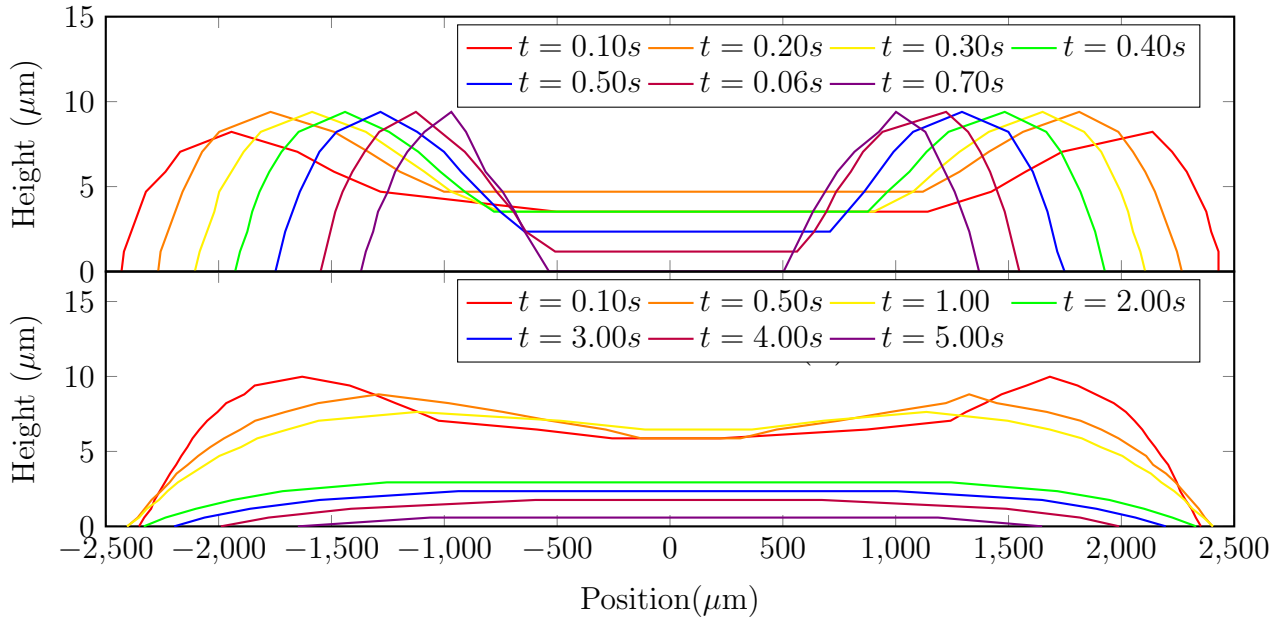

Figure 9: Evolution in time of drop profiles at time t after impact for temperatures (a) $T = 1.7991$ K and (b) 2.1495 K; note the longer time scale in (b). Retraction for colder drops was characterized by a constant contact angle (as can been seen by the parallel drop profiles in time), a radius that retracts linearly with time (shown by the equal linear distance in time between profiles), a constant height, a very short lifetime, and a 'donut hole' that forms in the middle of the drop as it drains. By contrast, drops near T_λ (which contain a very small fraction of superfluid), underwent a "deflation" where the drops appear to collapse on themselves as the fluid drains more slowly than with the colder drops.

microscopically thin adsorbed film which coats the substrate. Only the superfluid moves in the thin film because the normal component is viscously clamped to the substrate.

Another basic assumption is that in quasi steady state the pressure in the vapor at the liquid-vapor interface is constant and can be taken to be zero. The pressure inside the drop is mainly determined by three effects: the Laplace curvature, the van der Waals interaction potential of the fluid with the substrate, and the Bernoulli pressure term which is proportional to $-v^2$, i.e. a high flow velocity corresponds to a low pressure. The flow velocity v is not directly observable, but the superfluid flux $j = \frac{\rho_s}{\rho} v(x)\, h(x)$ is observable, where x is the coordinate along the substrate normal to the thin film-drop contact line, ρ_s/ρ is the fraction of fluid that is superfluid in the two-fluid model, and $h(x)$ is the height of the liquid-vapor interface. In steady state, j is constant, so v is inversely proportional to

the liquid thickness, with $v(x) = \frac{j\,\rho}{h(x)\,\rho_s}$. A Lagrangian which describes the difference between the kinetic energy of flow and the potential energy of the fluid is $L = (\rho_s/2)h(x)(\rho/\rho_s)^2 j^2/h(x)^2 - (\Delta\mu\, h(x) + \gamma\sqrt{1+h'(x)^2} + C\,d/(3h(x)^3)$. The Euler equation for this Lagrangian is

$$\Delta\mu = \gamma\, h''(x) + \frac{C\,d}{h(x)^4} - \frac{\rho^2}{\rho_s}\frac{j^2}{2h(x)^2}, \tag{10}$$

where the constants $C \sim 4.9 \times 10^{-22}$ J and $d \sim 14\,\text{nm}$ characterize the retarded van der Waals interaction, and $h'(x)$ is assumed to be small. The constant j can be determined from the rate of change of the drop volume. Assuming the drops are axially symmetric, integrating the drop profiles as shown in Figure 9 yields the drop volume V as a function of time, and then $dV/dt = 2\pi r\, j$ can be used to calculate j. The results are shown as a function of temperature in Figure 13, and a schematic of the drop on the surface is shown in Figure 10.

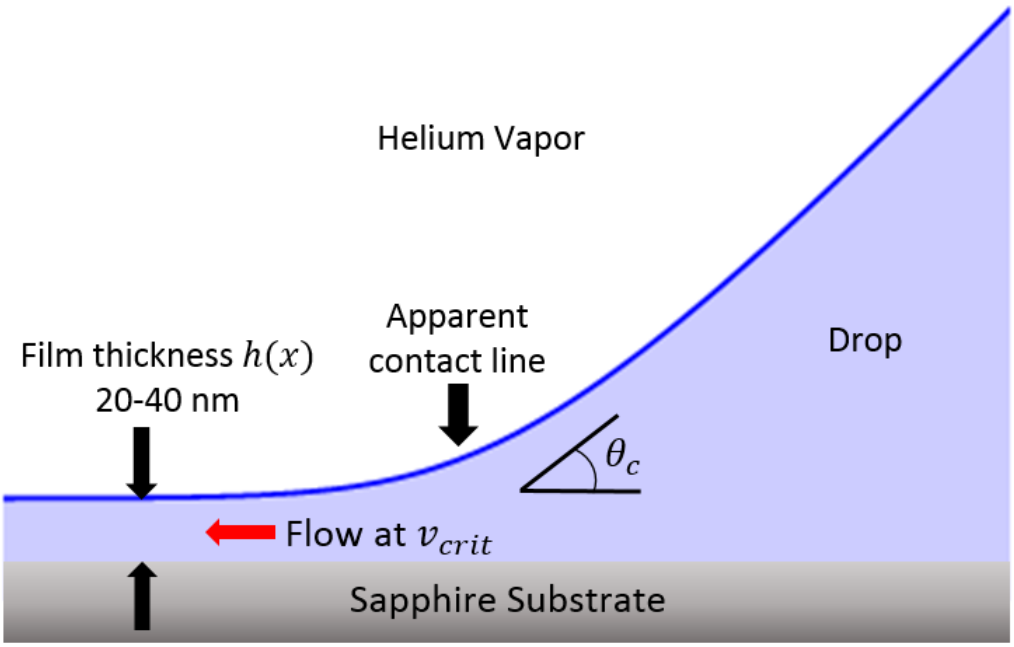

Figure 10: (Color online.) Cross-sectional schematic of a drop on the substrate showing superfluid flow out of the drop through the thin film at v_{crit}, film thickness $h(x)$, and contact angle θ_c. The pressure at the liquid-vapor interface is zero. The pressure in the thin film region is raised by the van der Waals force, but is lowered overall by the faster-moving flow.

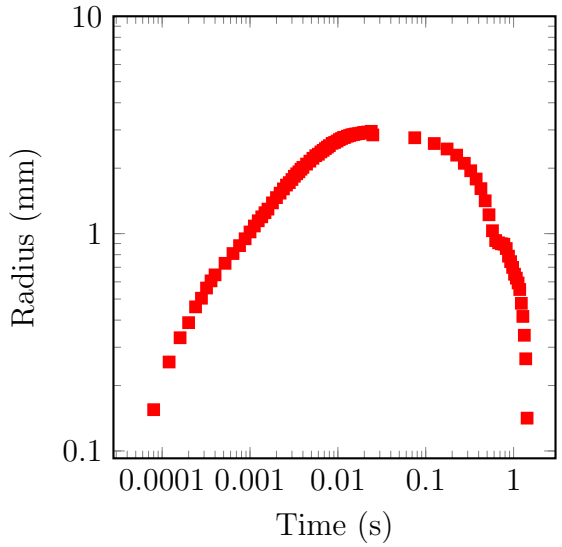

Figure 11: (Color online.) Total drop lifetime (radius vs. time) created by combining two drops filmed at different frame rates, with a drop at $T = 1.648$ K plotted here for the short-term spreading and a drop at $T = 1.626$ K plotted to show the two-phase contraction. The linear phase of the two-phase contraction appears curved here because this is a log-log plot.

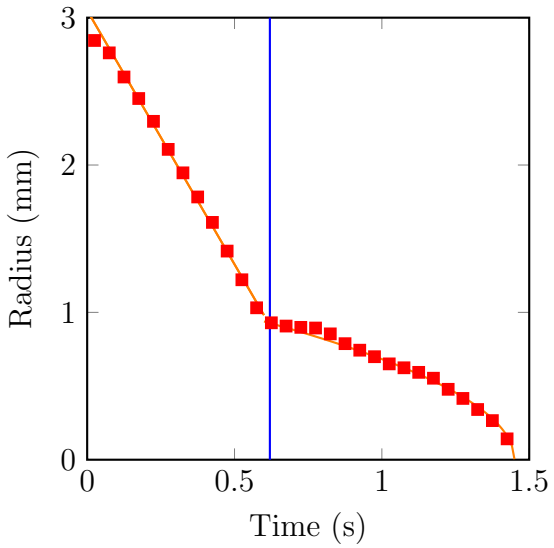

Figure 12: (Color online.) Radius vs. time for a retracting superfluid drop at $T = 1.626$ K. The linear behavior from 0 to 0.6 seconds corresponds to the retraction of the toroidal drops with constant contact line velocity. The change in behavior at $t = 0.6s$ (marked by the blue vertical line) is the transition to a spherical cap shape. The orange lines are fits for the data

Equation 10 describes the transition from a nanometer-thick film to a drop of bulk liquid, as illustrated in Figure 10. Neglecting $\Delta\mu$ and introducing a reduced height h_r with $h = h_r\sqrt{2C\,d\,\rho_s}\,(j\,\rho)^{-1}$ and a reduced transverse distance x_r with $x = x_r(2\rho_s)^{5/4}(C\,d)^{3/4}\gamma^{1/2}(j\,\rho)^{-5/2}$ yields a non-dimensional equation

$$h_r'' + \frac{1}{h_r^4} - \frac{1}{h_r^2} = 0. \tag{11}$$

This equation has a first integral

$$\frac{1}{3h_r^3} - \frac{1}{h_r} - \frac{1}{2}(h_r')^2 = const, \tag{12}$$

where the constant is determined by evaluating the expression in the flat thin film regime where $h_r = 1$ and $h_r' = 0$, so $const = -2/3$. For large h_r, equation12 yields

$h_r' \sim 2/\sqrt{3} + \mathcal{O}(1/h_r)$; this slope defines the contact angle of the bulk liquid drop as it merges into the flat adsorbed film. For small values of the slope, the contact angle θ_c in terms of dimensional parameters [27]is

$$\theta_c = \frac{2^{1/4}(j\,\rho)^{3/2}}{(3\gamma)^{1/2}(C\,d)^{1/4}\rho_s^{3/4}}. \tag{13}$$

The temperature dependence of j is measured in our experiment, and the temperature dependence of ρ_s and γ are tabulated [35]. A comparison of the predictions of Equation 13 and the values of θ_c measured from the interferometrically determined profiles is shown in Figure 14. Our measured values of θ_c agree very well with those of Poujade et. al [27], even though their measurements involved a static contact line formed by a plate immersed in the superfluid, while our contact line is dynamic. In both cases, the contact angle within a few milli kelvin below T_λ is remarkably high ($\sim 2^\circ$). Poujade et al. assumed that j had the same temperature dependence as the superfluid fraction. Our measurements show that the temperature dependence of j is more rapid than the superfluid fraction. For example, at $T = 1.9$ K, j has reached its asymptotic maximum low temperature value (which roughly agrees with the value assumed by Poujade et al.), but the superfluid fraction is less than 0.6. The model which generates the contact angle formula given by Equation 13 yields the right order of magnitude, but it does not seem to explain the temperature dependence correctly.

8 Conclusion: Superfluid Spreading

We have investigated the impact and spreading of superfluid helium drops on a sapphire substrate using video imaging and interferometry. The spreading rate of classical liquids is inversely proportional to the viscosity, so one of our initial goals was to see if the zero-viscosity superfluid spreads differently than the finite-viscosity normal fluid. We observed that the short-term (inertia-driven) spreading of the superfluid is not remarkably

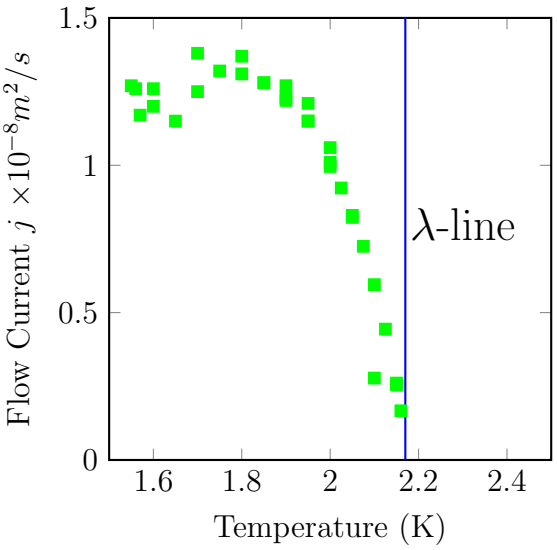

Figure 13: Flow current j as a function of temperature, calculated from drop lifetime.

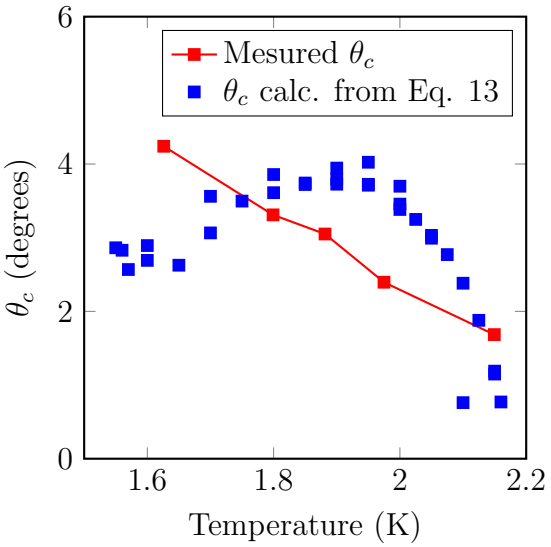

Figure 14: Comparison of interferometric measurements of θ_c as a function of temperature in red with the theoretical prediction of Equation 13 in blue.

fast, but is in fact very similar to the normal fluid because this portion of the spreading is dominated by the balance between the fluid's inertia and surface tension rather than by viscosity. The kinetic energy of the impact is dissipated in about 10 milliseconds even at temperatures where the superfluid fraction is greater than 0.95. Even though helium completely wets all conventional substrates, superfluid drops do not continue to spread with power law dynamics as most other fluids do. After the inertia-driven phase, superfluid drops do not spread at all, but rather contract and disappear. The lifetime is strongly temperature dependent and ranges from a few seconds at low temperatures to tens of seconds near T_λ. This lifetime is consistent with a model in which the superfluid flows out of the drop through the pre-existing nanometer scale adsorbed film on the substrate . The flow velocity in the film required to explain the drop lifetime is of the order of 1 m/s, which is similar to the critical velocity observed in other nanometer scale superflows. The contracting superfluid drops have a receding contact angle of several degrees. The existence of a finite contact angle as well as its approximate magnitude is explained by a model which balances surface tension, van der Waals forces and the Bernoulli pressure in the high

velocity flow in the thin film.

9 Introduction: Leidenfrost

When a freely falling liquid drop is incident on a solid horizontal surface, our intuition suggests that the drop should impact on the surface, spread out, and wet the surface in accordance with the contact angle θ_c. Under certain conditions, the dynamics of the vapor layer between the drop and the surface may impede or prevent this wetting, and under such conditions, the drop will levitate above the surface. There are three conditions induced by the vapor layer that can cause levitation: vapor film squeeze-out, the Leidenfrost effect, and the Marangoni effect. In this paper we explore all three possibilities, as the cause of levitation for our helium drops was not immediately obvious when we first observed it. We discovered these levitating drops during an experiment examining the impact and spreading of helium droplets. The levitation effect was observed when heat was applied to the impact surface at temperatures of 3.7-4.3 K, and surprisingly was observed with no heat input at temperatures of 4.3 K to 5.2 K, with 5.2 K being the critical temperature of helium. The observation was startling because the drops levitated with a very small temperature difference ΔT. An additional mystery was that our drops levitated in an atmosphere of only their own vapor (a one-component system) whereas nearly all other observations of drop levitation in the scientific literature have occurred with a fluid in air; this is significant because the air suporting conventional liquid drops is non-condensable, whereas the helium vapor supporting our helium drops is condensible. To our knowledge, ours is the first observation of Leidenfrost of a fluid in its own saturated vapor. Our motivation for conducting this experiment was to determine which of these three mechanisms was causing the levitation and to characterize it, because the levitation mechanism was mysterious to us upon first observation. We show quantitatively in this paper the leviation is best explained by the Leidenfrost effect.

10 Experimental Setup

The constraints of the experiment present a number of engineering challenges. Cryostats are typically employed for experiments in the temperature range of 1-5 K, which is the temperature range for this experiment. The cryostat must have windows which give optical access from the side so that high-speed video of the impacting drops can be taken. A method for delivering liquid helium drops both continuously and on demand must be used. The pressure inside the cell must be measured to ensure that cell environment remains at saturated vapor pressure. The temperature of ambient gain in the cell and the temperature of the drop impact surface must also be measured.

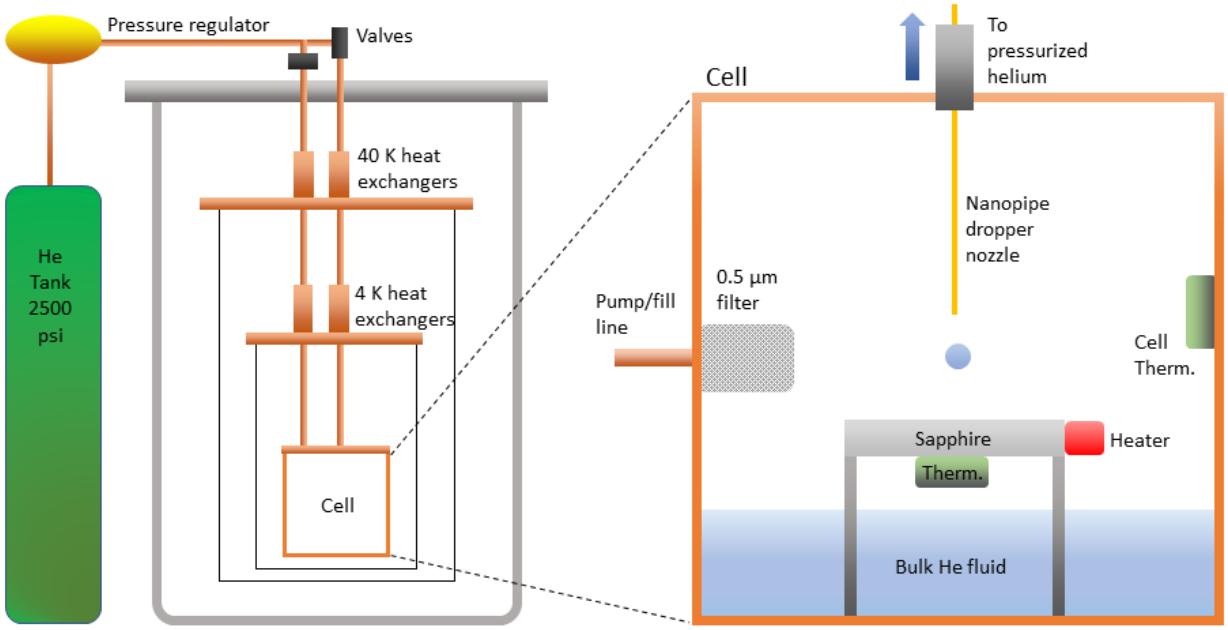

Figure 15: (Color online.) Experimental Setup. On the left is the overall setup with the cryostat, helium tank, and lighting and camera setup. On the right is a magnified view of the cell, which includes the nanopipe dropper, sapphire impact surface, thermometers, heaters, and bulk liquid.

The experimental setup is shown in Figure 2. The cryostat is constructed in the manner of a set of Russian dolls with an outer region held at a temperature of 40 K, an inner region held at about 4 K, and a cell (which contained the experiment) that could vary in

temperature between 1.2 K and 10 K. The temperature in the cell was controlled by a heater linked to a PID loop controlled by a Lakeshore 366 cryogenic temperature controller. The entire cryostat, except for the experimental cell and the helium fill and drain pipes attached to it, was kept at high vacuum at a pressure $p < 10^{-6}$ Torr. The helium drops were delivered by a glass nanopipe with an inner diameter of 10 μm and an outer diameter of 365 μm, and the impedance of the tube was $3.105 * 10^{20}$ m^{-3}. These drops were squeezed out by a pressurized helium tank external to the cryostat that was regulated by a pressure regulator and a needle valve. The impedance allowed the dropper input line to be pressurized and to stay at a stable pressure while regulating the flow of helium. If the proper pressure was applied to the dropper input line, the drops would fall from the dropper at predictable intervals. To obtain drops from the dropper line, helium was put in the line to a pressure of 2-50 Torr above saturated vapor pressure, depending on the desired drop frequency.

The impact surface was a cylindrical piece of sapphire 1" in diameter and 3 mm thick. A small ohmic heater with superconducting leads was glued onto the side of the sapphire to provide the ΔT for levitating the drops. A heater was attached to the bottom of the sapphire to measure its temperature, and another thermometer was mounted on the inner wall of the cell to measure the cell's ambient temperature. The very high thermal conductivity of sapphire at low temperature ensured that thermal equilibrium within the sapphire impact surface and attached heater was nearly instantaneous. The impact surface thermometer was calibrated against the cell wall thermometer, and the two thermometers agreed to within 1mK. An LED light was used to illuminate the impact surface so as to be seen by the high-speed camera, and at temperature above 4.2 K, the ΔT of 1-2 mK provided by the light alone was usually sufficient to levitate the drops. The camera used for imaging from the side was mounted at a downward angle of about 4 degrees. A second pump line with a filter was used to add or remove helium from the cell independent of the dropper line.

The temperature of both thermometers was measured by the temperature controller at a rate of 100 samples per second. This allowed for good accuracy in measuring the ΔT in real time. Typical power inputs (provided by an external DC power supply) needed to levitate the drop were 0 mW for temperatures above 4.2 K to 64 mW for 3.68 K. A typical temperature curve for the impact surface and ambient cell is shown in in Figure 16. When power was applied, the temperature of the impact surface would quickly rise faster than the cell, and then the temperatures of the impact and surface would rise in parallel, which kept the ΔT between the two relatively constant.

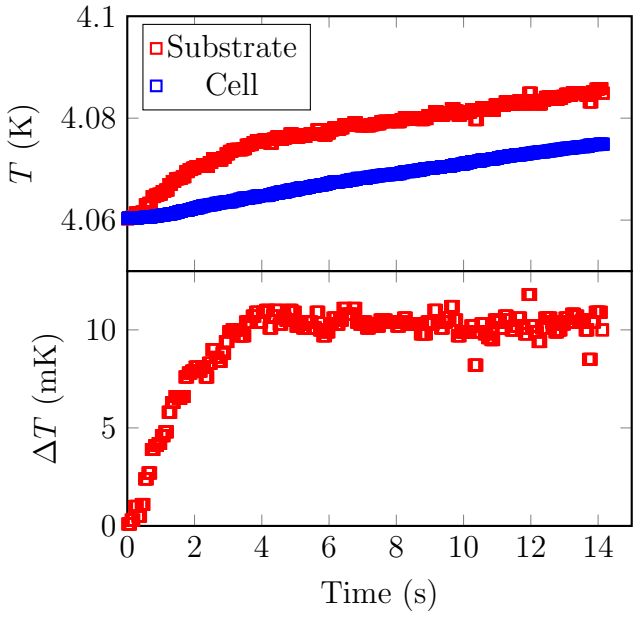

Figure 16: (Color online.) Temperature profile of the experiment at a power input of 14 mW. (a) shows the cell and substrate temperatures over this time period, and (b) shows ΔT, the difference between the two. When the power input begins at time $t = 0$, the substrate temperature rises faster than the ambient cell temperature for a few seconds; then thermal coupling of the substrate and the ambient gas cause the two rise together in parallel, maintaining a reasonably constant ΔT.

To measure the ΔT needed to levitate a drop, the dropper was set with backpressure so as to deliver about 1 drop per second; while the dropper was delivering drops at a constant rate, the power supply to the impact surface was turned on and the temperature controller took 100 temperature measurements per second of both the impact surface thermometer

and the cell thermometer. The high-speed camera was used to visually monitor the impacting drops on the surface in real time. As soon as a drop was observed to levitate, the temperature measurement sampling was stopped, and the temperature of both the impact surface and the cell was recorded; the temperature of the surface at this point was taken to be T_L, the temperature of the cell was taken to be T, and the difference between the two was taken to be ΔT.

11 Results and Discussion: Leidenfrost

Images of our helium Leidenfrost drops are shown in Figure 17; the images demonstrate that the effect is very robust. As previously stated, it was initially unclear to us what mechanism might be causing the drops to levitate when levitation was first observed. In this section we present our experimental data and we discuss the three possibilities (vapor film squeeze-out, Marangoni, effect, and Leidenfrost effect) we considered in trying to determine the mechanism that was responsible for levitation. Figure 18 shows the primary data for levitation as a function of temperature, and Figure 19

11.1 Vapor Film Squeeze-Out

One mechanism by which drops may levitate is film squeeze-out, where vapor trapped between the drop and the surface must exit before liquid-surface contact can be made. This has been modeled as parallel-plate squeezing, where two flat parallel plates are squeezed together with the vapor in between. The incompressibility of the gas dictates that the vapor must take time to escape, and the drop may levitate for the amount of time that the vapor is being squeezed out. The time for the squeeze out is given by the well-known equation

$$h = \frac{3h_0\sqrt{\mu_v}R_d^2}{\sqrt{9\mu_v R_d^4 + 16h_0^2 R^3 t\rho}}. \tag{14}$$

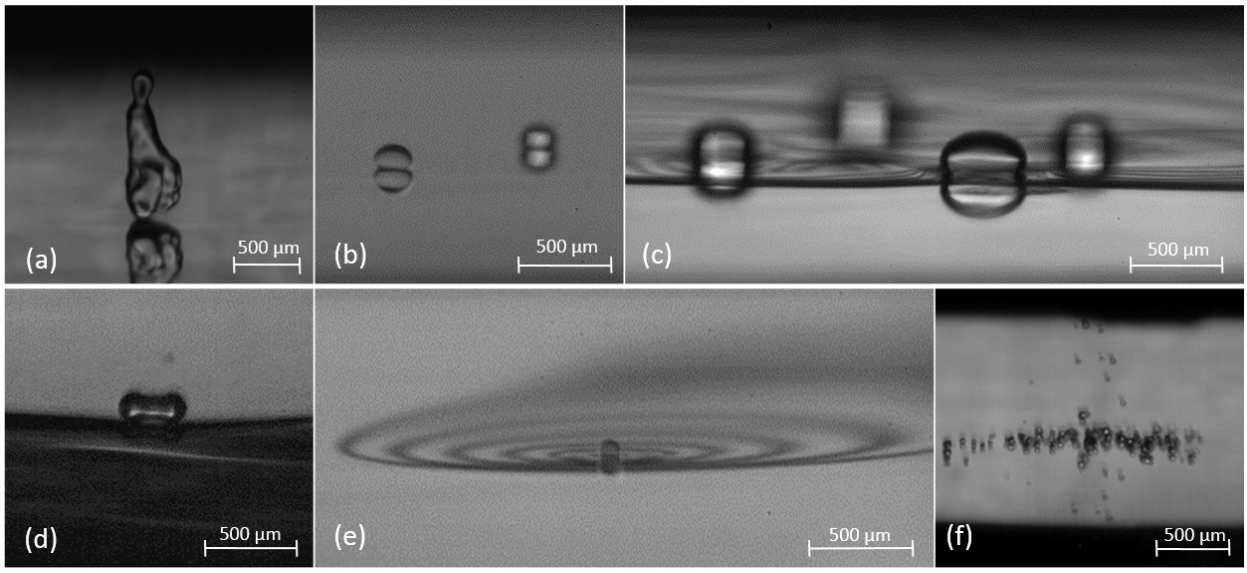

Figure 17: The many faces of Leidenfrost in liquid helium. (a) shows a drop rebounding from a dry surface. (b) shows two drops (the further one is beyond the depth of field of the microscope) levitating on a dry surface near the critical point at 5.108 K; these drops are very small because the surface tension becomes very small near the critical point. (c) shows drops levitation on liquid at 4.88 K; the foreground of the image is the dry surface. (d) shows two levitating droplets coalescing with each other, but not with the dry surface (background) or the wet surface (foreground) [1]. (e) shows a droplet at 5.19 K, very near the critical point; the droplet is extremely small because of very low surface tension, and it levitates on a thin pool of liquid helium. The light and dark fringes are interference lines, with each fringe (light to light or dark to dark) representing a change in height of 1167 nm. (f) shows "baby" droplets levitating on a dry surface after being sprayed out of a heated nozzle.

with drop radius R, drop height above the surface h, initial drop height h_0, vapor dynamic viscosity μ_a, reduced radius $R_d = R^2/l_c$ (capillary length l_c), fluid density ρ, and elapsed time t. The parallel plate model suggests that we would need to wait forever to reach contact at $h = 0$; but in reality, vibrational modes and other motion within the drop are likely to cause the drop to deviate from this model and cause parts of the drop to move closer to the surface and cause contact and wetting. Our high-speed videography observations of levitating helium drops that do not appear to be Leidenfrost drops (at temperatures below T_L) show that these drops levitate for about 3-30 ms before wetting the surface, suggesting (by Equation 14) a failure of the supporting film at 30-100 nm, in the regieme where van der Waals forces can cause film failure for levitating drops [36]. If

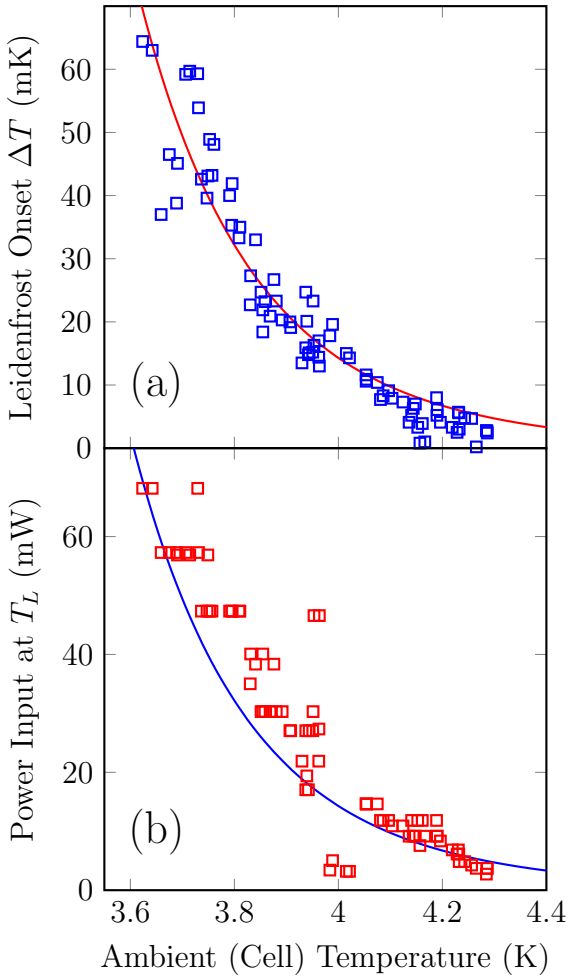

Figure 18: Leidenfrost onset ΔT is shown in (a) as a function of cell temperature. At lower temperatures more power input is needed to levitate the drops, and at higher temperatures the light from the LED was enough to produce the 1 mK of ΔT needed for levitation. (b) shows the power input needed for levitation as a function of cell temperature, with much less power input needed to levitate the drops at higher temperatures. Above a temperature of 4.3 K, all drops levitated with no power input from the impact surface heater because the light from the LED provided sufficient ΔT to levitate the drops.

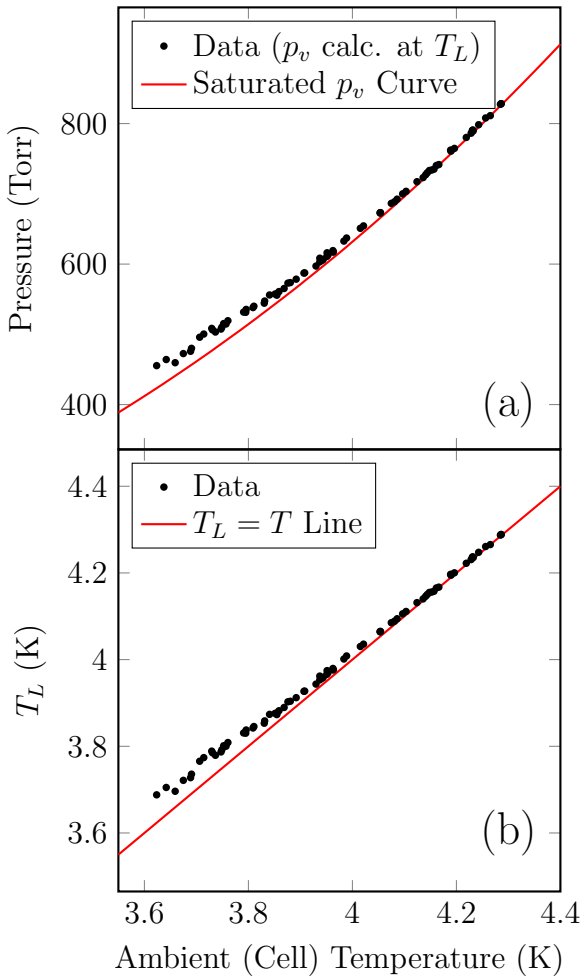

Figure 19: (Color online.) (a) shows the calculated vapor pressure of a drop at the temperature of the heated surface required for leviation; this is given as a function of cell temperature. (b) shows T_L (which is the sum of cell temperature and the ΔT needed for levitation) as a function of cell temperature in comparison to a line $T_L = T$. The plot shows that the difference between T_L and T gets smaller as the temperature gets higher.

levitation lasts longer than 3-30 ms, other forces must be responsible for levitation. Additionally, Figure Equation eq:filmcompress does not suggest temperature dependence for leviation other than a very small effects caused to temperature-dependent changes in viscosity and density as a function of temperature. Thus, vapor film squeeze-out would not adequately explain the temperature dependence of ΔT shown in Figure fig:dtandpowervst.

11.2 Marangoni Effect and Supporting Film Squeezing

We consider whether or not this helium levitation can be explained by the Marangoni effect, wherein a small temperature gradient within the drop creates thermocaplliary flow, dragging the ambient gas underneath the drop, causing levitation. Marangoni-driven levitation has been observed to occur at much lower ΔTs than Leidenfrost, [37, 38], and seems like a candidate to explain the small ΔT needed for helium drop levitation. The Marangoni effect is mass transfer that is driven by a gradient in a fluid's surface tension. In the case of fluids where surface tension is dependent temperature, a surface tension gradient may be induced by a temperature gradient. The effect is strong enough to create drop levitation when a temperature gradient in a drop causes circulation inside the drop induced by the resulting surface tension gradient; this circulation within the fluid causes adjacent gas to be pulled under the drop, supporting the drop's weight. The threshold above which levitation due to the Marangoni effect may occur is determined [37] by the dimensionless Marangoni number Ma, which is

$$Ma = \frac{|\sigma_T \Delta T_0| R}{\mu_0 \alpha_0} \tag{15}$$

where σ_T is the derivative of the surface tension with respect to temperature, and $\alpha_0 = k/\rho C_P$ is the thermal diffusivity, with heat capacity at constant pressure C_P. Levitation can occur if $Ma = 100 \pm 50$. In our drops, this would require a temperature difference of 200μK, which seems plausible in our cell.

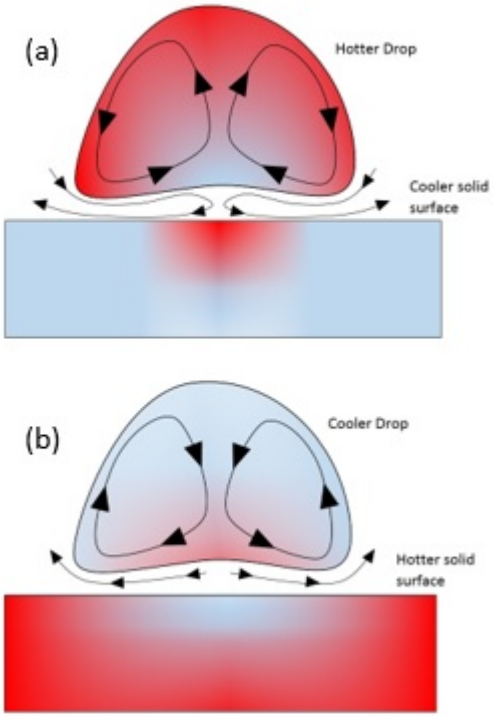

hb!

Figure 20: In Marangoni levitation, the drop's weight is balanced by the additional pressure of external gas dragged underneath the drop by the internal fluid motion. (a) shows a schematic of a hotter drop levitating over colder surface. The drop and the surface each induce a temperature gradient in the other as shown; this causes a surface tension gradient within the drop which drives an internal circulating flow, dragging the ambient gas under the drop and supporting it. (b) shows a schematic of the scenario of a colder drop and a hotter surface; the flow in this case drags the flow out from underneath the drop, so the drop will not levitate.

The question is easily answered in the negative for levitation over a solid surface, but is more difficult for levitation over a liquid. For levitation over a solid surface, the drop must be hotter than the surface to ensure that the vapor flow is in the proper direction for levitation; in the case where the surface is hotter than the drop, the thermocapillary flow will drag the vapor away from the bottom of the drop [39, 40], causing the drop to wet even faster (illustrated in Figure 20.) We performed an additional run of our experiment wherein we used the dropper nozzle heater to heat the droplets before they fell, ensuring that the drops were hotter than the substrate. Even with up to 100 mW of heat input, no drop levitation was observed for any cell temperature, suggesting that drops will levitate only if the surface is hotter than the drop. Additionally, our levitating drops roamed freely between the liquid and solid surfaces, suggesting that the levitation mechanism was the same for both the solid surface and the thin liquid pool.

11.3 The Leidenfrost Effect

The Leidenfrost effect, wherein a droplet of fluid is levitated above a hot surface on a cushion of its own vapor, has been studied extensively with a variety of fluids on a variety of surfaces under different experimental conditions
[41, 42, 2, 43, 44, 45, 46, 1, 37, 47, 38, 48, 49, 40, 50, 51], and several theoretical models have been proposed [52, 36, 53, 54, 55]. Notwithstanding this abundance of research, several mysteries remain, including the relationship between the minimum temperature difference ΔT necessary for levitation onset and the properties of the fluid and surface. Additionally, the vast majority of this research has taken place in an environment of air at room temperature. A few authors have studied Leidenfrost at pressures lower than atmospheric pressure [42, 51] and at pressures higher than atmospheric pressure [43], but little or no literature exists for Leidenfrost drops in coexistence with its own vapor, which is the subject of our experiment.

In spite of a large body of research into the Leidenfrost phenomenon, there is no generally

accepted predictive formula for the Leidenfrost onset temperature T_L, or temperature difference ΔT between the surface and the fluid drop, as a function of the parameters of the fluid, surface, and environment; and still much about the T_L remains mysterious [56]. Some models, including those of Testa and Nicotra [42] and Orejon et al. [51] found that T_L for water at ambient pressures below 1 atmosphere varies along a curve that is loosely parallel to the vapor pressure curve. Other models give a T_L that is independent of the temperature of pressure of the fluid or the environment; these models are of much less use to us than the models that account for variations in temperature and pressure. They also do not link T_L to the onset of film boiling, which is the process by which a Leidenfrost drop levitates. In light of this, we discuss or motivation for the experiment.

There is currently no consensus about what precisely determines ΔT and T_L. We attempt to show here that a very small value ΔT is reasonable for liquid helium, though it remains mysterious why water and other fluids require a much larger ΔT to initiate Leidenfrost levitation. We calculate the ΔT needed to levitate the drop by starting with the principle that a liquid in equilibrium with its own saturated vapor (at any temperature) is already at its boiling point. Along the saturated vapor pressure curve, a small change in temperature will give rise to a large change in vapor pressure, and only a few pascals are needed to support the weight of the drop and produce levitation. We calculate that the drop needs to be only μK hotter than the ambient temperature to balance the force of gravity. the drop. A few authors have found that drop non-coalescence occurs with a very small T_L. Weilert et al. [57] discovered that helium drops levitating in a magnetic field would not coalesce with each other when the drops were cooling off due to evaporative cooling; in this case, the ΔT was also very small, on the order of microkelvins. Maquet et al. [1] found that they could levitate a drop of ethanol on top of a pool of silicon oil at a ΔT of only 1 K, and determined that this was Leidenfrost.

Figure 18(a) shows our results for the minimum temperature difference ΔT needed to levitate a drop as a function of the ambient temperature in the cell at saturated vapor

pressure. Figure 18(b) shows power input to the substrate that is required for the onset of Leidenfrost as a function of the cell temperature. The plot in Figure 19(a) is somewhat tricky; each data point shown in the calculated helium vapor pressure p_v from each data point for T_L measured at each cell temperature, along with the saturated vapor pressure curve. Figure 19(b) shows T_L vs T, with the red line indicating $T_L = T$. The vertical axis represents he minimum temperature difference ΔT in millikelvin needed to levitate a drop at corresponding ambient temperature T. The curve runs inversely proportional to the vapor pressure. We did not observe any Leidenfrost drops at all below a temperature of 3.6 K, even with hundreds of milliwatts of heat input. Above a temperature of $T \sim 4.2K$, all drops levitated, largely because the light used to illuminate the impact surface produced a ΔT of about 1 mK, which was enough to levitate the drops. Our temperature resolution was only valid to within 1 mK, so smaller values of ΔT were not measurable for this experiment. The experiment was carried all the way to the critical point of 5.2 K, and the drops continued to levitate all the way to the critical point with a ΔT of less than 1 mK. The plot in Figure 19(a) looks similar to Emmerson's plots [43] wherein T_L approaches the vapor pressure curve as the temperature approaches the critical temperature. We also note that Emmerson's Equation 3 does not hold for liquid helium, as it was found that it does not hold for water [43].

11.4 Vapor Layer Thickness

Several factors made it very difficult to obtain an accurate empirical measurement of the supporting vapor layer thickness, including the location of the experiment inside the cryostat, the thinness of the vapor layer, and the low index of refraction of liquid helium. Additionally, the internal temperature of the drops is also very difficult to measure given the constraints of the experiment inside the cryostat and the small size of the drops. We present a model here for calculating the internal temperature of the levitating drops and the vapor layer thickness on which they levitate. We characterize the system with ambient

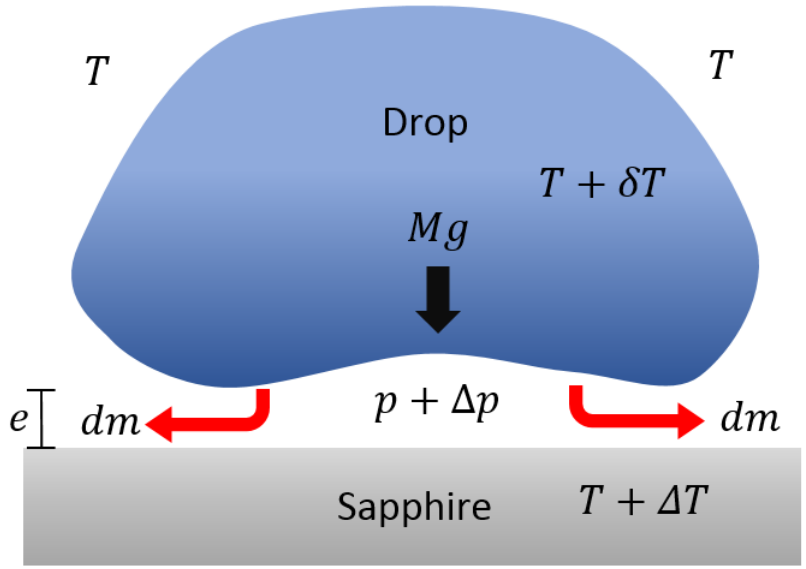

Figure 21: (Color online.) Schematic of a Leidenfrost drop levitating above the sapphire substrate. The sapphire is hotter than the drop, and heat is transferred to the drop through the vapor layer with thickness e. The drop's weight Mg is supported by the pressure Δp of the additional gas that is evaporating from the drop, and the drop loses mass dm in time dt as the gas escapes.

(cell) temperature T, a drop levitating above a surface at height e and at an internal temperature of $T + \delta T$, a (heated) surface with a temperature of $T_h = T + \Delta T$, an ambient pressure of P, and a pressure underneath the drop of $P + \Delta P$. Mechanical equilibrium requires that the average pressure $\Delta P/2$ multiplied by the drop area A needs to balance the gravitation force of the drop, so $\Delta P = 2Mg/A$, with drop mass M and gravitational constant g. The pressure drop exists because of viscous flow of the vapor emitted by the drop, which is characterized by a mass flux J. The standard lubrication approximation neglects the inertial terms and balances the pressure drop against viscous forces. Assuming velocity v goes to zero at the boundary of the substrate and the drop, the mass flux J is $J = \rho v_r(r)$ with velocity v_r being the velocity as a function of radial position. The flux is proportional to the area behind a ring,

$$2\pi r \rho v_r(r) = J\pi r^2 \tag{16}$$

which implies that $v(r) = v_0 r$. Conserving mass and finding the average velocity across the gap,

$$2\pi\rho re \int \frac{-e^2 \frac{dP}{dr} + z^2 \frac{dP}{dr}}{2\nu\rho} = J\pi r^2 \tag{17}$$

why gas dynamic viscosity ν. Solving this equation yields

$$\frac{dP}{dr} = -\frac{3Jr\nu}{2e^3} \tag{18}$$

The mass flux J is

$$J = \frac{\sqrt{3m}\frac{dP}{dT}}{\sqrt{k_b T}} \tag{19}$$

The number flux is nc, with $c = \sqrt{3k_b T/m}$ and $n = N/V = p/k_b T$ using the ideal gas law, with volume V, Boltzmann constant k_b, and pressure p. Evaporation is driven by the difference in pressure between the two phases. Along the saturated vapor pressure curve, a small change in temperature will give rise to a rather large change in pressure. We use the vapor pressure p_{vap} of helium,

$$p_{vap}(T) = e^{(10.4385 - \frac{7.59649}{T})} T^{1.99793} \tag{20}$$

The pressure drop exists because of viscous flow of the vapor emitted by the drop, which is characterized by mass flux J. The pressure drop ΔP is

$$2\frac{Mg}{A} = \frac{3r^2\nu}{2e^3} \frac{\sqrt{3m}\frac{dp_{vap}}{dT}\delta T}{\sqrt{k_b T}} \tag{21}$$

We have one equation and two unknowns, so we need an additional equation, this one involving heat transfer. δT is determined by the heat transfer from the hot surface. The heat flux q from the hot surface to the drop is $\kappa(T_h - T)/e$. Because the drop is slightly hotter than its surroundings, it will evaporate, which will remove heat from the drop at

rate $J * L$ with latent heat L per unit mass. We balance the heat going into the drop and coming out of the drop,

$$\kappa \frac{T_h - T}{e} = \frac{\sqrt{3m}\frac{dp_{vap}}{dT}\delta T}{\sqrt{k_b T}} L \tag{22}$$

We now have two equations and two unknowns; solving Equation 21 and Equation 22 as a system of equations, we are able generate predicted values for δT and e using our data for ΔT as shown in Figure 18(a). When we solve these same two equations and use the data for the Leidenfrost in water at room temperature, we obtain a δT of 906 μK and a vapor layer thickness e of 40 μm, which is in good agreement with experimental data for water [2, 45, 46]; this gives us increased confidence in the accuracy of this model.

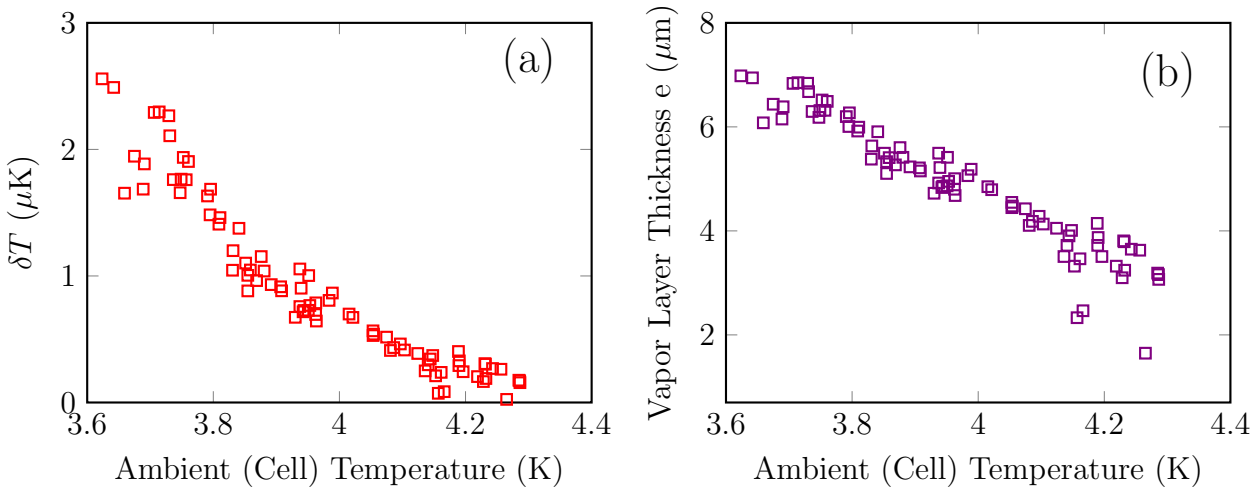

Figure 22: (Color online.) Predicted internal temperature difference δT is shown in (a); this was calculated by using the data shown in Figure 18 and Equation , and (b) shows the vapor layer calculated by the same method.

One of the unsolved mysteries of T_L is why it is so much larger than seems necessary to levitate drops. Indeed, only about 1 K of ΔT is needed to increase water's vapor pressure by the few pascals required to levitate a water droplet, so it remains unclear why many

years of experimental evidence have demonstrated that water does not levitate above solid surfaces until $\Delta T \sim 115$ K. We can make a rudementary calculation of the ΔT needed to levitate a drop of water by balancing the weight mg of the drop against the supporting force pA underneath, from this we get $\Delta p = 4gR\rho/3$; for a water droplet of radius 2 mm, the Δp needed for levitation is very small, about 13 Pa; this 13 Pa difference can be produced with only about 100 mK of ΔT. It remains mysterious why Leidenfrost levitation is not thus much more common on everyday surfaces at room temperature. However, we have produced Leidenfrost for such very small values of ΔT in our helium experiment. Biance et al. [2] devised a forumla for the vapor layer thickness e by balancing the heat-driven evaporation from the drop with the Poiselle flow out of the bottom of the drop, starting with

$$\frac{dm}{dt} = \frac{\kappa}{L}\frac{\Delta T}{e}\pi\lambda^2, \tag{23}$$

with mass differential dm, time differential dt, vapor layer thermal conductivity κ, fluid latent heat L, temperature difference between the substrate and the fluid (at its boiling point) ΔT, vapor layer thickness e, and surface area under the drop $\pi\lambda^2$. Using this as a starting point, we solve the differential equation with the initial condition that the mass of the drop at lifetime τ is 0, then use the condition that the mass of the drop at time $t = 0$ is ρV (fluid density times volume), and we get

$$e = \frac{\Delta T \kappa \tau}{4LR_0\rho}, \tag{24}$$

with initial drop radius R_0 and fluid density ρ, and substituting our values for helium we get $e \sim 700nm$. This value of e is too small to measure using laser interferometry and difficult to measure using frustrated total internal reflection (TIR) [58, 47]. It may be possible to measure it using two-color interferometry, but the relatively faint reflected waves caused by the low index of refraction for liquid helium makes this difficult. The

following table shows the calculated vapor thickness values e, based on the formulas given and formula sources.

11.5 Droplet Lifetime

Many (and sometimes most) of the drops impacting on the surface above T_L did not levitate, particularly at temperatures between 3.5 - 3.9 K. We account for this by observing that the very thin vapor film supporting the drop was subject to failure due to thermocapillary forces and van der Waals forces [36]. Although some authors [41, 48, 49] observe the final destiny of Leidenfrost droplets to be be either take-off (because of the failure of the lubrication approximation) or explosion (because of the failure of the vapor film), neither of these were observed in our helium droplets. The drops met their demise either by shrinking to the point of disappearing, or by wetting the surface before fully shrinking, often undergoing a coalescence cascade [3] and frequently causing further Leidenfrost with the daughter droplets, as shown in Figure 24. The absence of take-off can be explained by observing that the lubrication approximation fails when $h \sim l$, and since $h \sim 700nm$ for our drops, the drops need to be extremely small to take off, smaller than the resolution of our camera. Exploding drops were not observed because the ΔT between the surface and the drop is too small. The histogram in Figure 23 shows the levitation of 25 drops impacting on the surface above T_L

Our longest drop lasted 34 seconds, and this drop was levitated with $\Delta T < 1$ mK. Drop lifetimes were shorter when more heat was applied to the impact surface. To measure the droplet lifetime, the high-speed camera was used at a rate of 100 fps to record video of impacting drops, and from this video, the lifetime of each drop, and its radius as a function of time, could be measured.

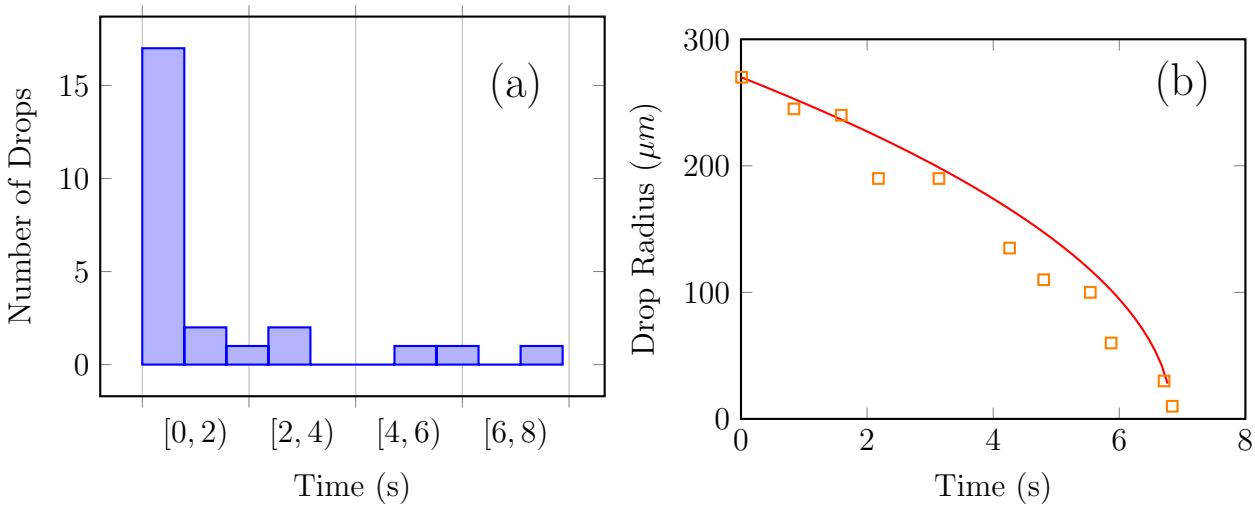

Figure 23: (Color online.) The histogram in Figure (a) shows the number of drops in each lifetime range for a set of 25 drops. (b) shows a typical drop whose outer radius (plotted here) shrank all the way to zero before wetting the surface. The fit shown is $R(t) = R_0(1 - \frac{t}{\tau})^{1/2}$, similar to experiments for water at room temperature [2]. The power input here is 58 mW.

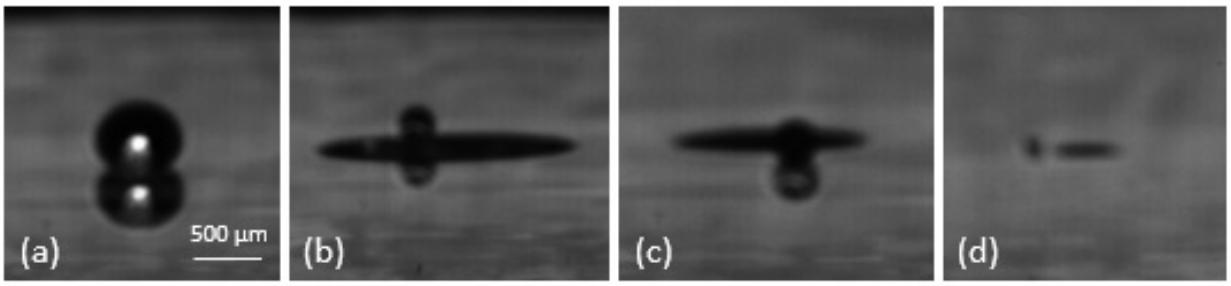

Figure 24: The "Leidenfrost Cascade." The whole drop (a) levitates for a few seconds before beginning the coalescence cascade [3], producing a daughter drop which levitates on the liquid puddle (b). The daughter drop rolls off the puddle onto the solid surface and continues to levitate while the puddle evaporates (c). This daughter drop continues the coalescence cascade, producing an even smaller puddle and smaller drop that continues to levitate (d).

11.6 Relationship with Film Boiling Onset

Previous experiments have shown that T_L for water coincides with the onset of film boiling (these experiments are usually carried out with a conductive wire immersed in a fluid bath) in accordance with the boiling curve for water [59], with $\Delta T \sim 115K$ above the saturation temperature T_{sat} (or boiling temperature) T_{sat}. An analogous experiment by Goodling and Irey [60] showed that the onset of film boiling in helium occurs at a temperature of about 2 K above T_{sat}, and based on this, Baumeister and Simon [55] predicted a T_L for helium of

4.2 K. Steward [61] found that film boiling onset in helium occurs at a ΔT of about 1 K. If, as with water, T_L for helium coincides with the onset of film boiling, we should observe that a ΔT of 1-2 K will be necessary to levitate the drops; this is the primary subject of our investigation. However, our experiments have shown both that ΔT for helium is much smaller than the boiling curve of helium would predict, and also that T_L varies with temperature. Film boiling in liquid helium is of particular interest to engineering applications in which liquid helium is used to cool equipment, as the onset of film boiling is a failure mode of such cooling applications. Film boiling onset is also of interest in thermal management systems for spacecraft and has been studied in microgravity [62, 63].
The boiling curve for water is well-known, and it is well-established that the T_L in water coincides with the onset temperature of film boiling. However, boiling curves for other fluids are not as well-established, and is is not known whether T_L always coincides with the onset of film boiling in a standard boiling curve. Our results, and the results of Maquet et. al. who found that a drop of ethanol could levitate on a pool of silicon oil far below the temperature for the onset of film boiling [1] suggest that it does not. One possibility to explain the very small ΔT is that the very high thermal conductivity of sapphire at low temperature creates a highly isothermal surface on which to levitate; this is in contrast to more conventional surfaces at room temperature, which may be cooled substantially by the incident drop [45]. Further support for this is found in the change of levitation time for a drop of ethanol levitating on a pool of silicon oil as a function of the oil viscosity [1], indicating that thermal activity in the substrate affects T_L.

11.7 Levitation Over Liquid

A surprising finding was that the drops would levitate both over a dry surface and a wet helium puddle up to tens of micrometers deep, even though the wet surface did not seem to be undergoing any boiling, and was ostensibly the same temperature as the solid. In fact, the levitating drops wandered freely between two, with the ability to crawl or roll from the

dry surface onto the wet surface, or vice versa, with ease. The wet surface was capable of supporting large drops with at least 4 times the volume of a standard-size drop. Macquet et al. [1] showed that a drop can levitate over a pool of another fluid with a very small ΔT, and also showed that two drops levitating on a surface may coalesce with each other while not coalescing with the surface.

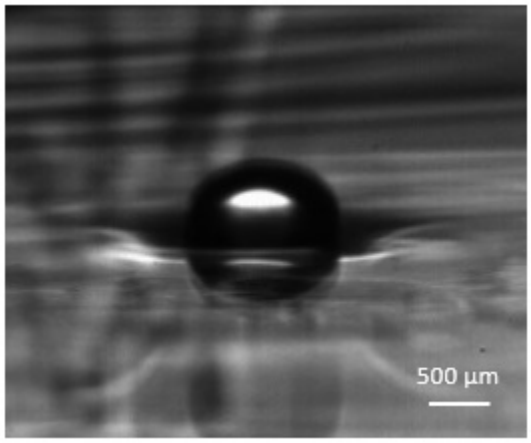

Figure 25: This larger levitating drop was formed from three smaller droplets that coalesced, and lasted for several seconds. The liquid pool is tens of micrometers thick and exists on top of the sapphire substrate. The heat input is 8 mW.

Levitation over a liquid is shown in Figure 25, and also in Figures 17(c) and 17(e). Macquet et al. [1] showed that a drop of fluid can levitate over another fluid for a very small ΔT, and also showed that the liquid pool deforms under the weight of the drop. Our drops behaved similarly, with liquid pool deformation and a very small ΔT needed for levitation, though it is not clear at present that the ΔT for levitation over liquid is smaller than that needed over the solid substrate. Thin liquid layers on the sapphire were created in our experiment when the substrate was allowed to sit in the vapor without heat input; liquid also formed on the surface when the dropper was allowed to run continuously with no heat input, forming a large puddle. This fluid layer was tens of micrometers thick, and the drops were observed to levitate on this easily with minimal heat input, and sometimes with no heat input.

12 Conclusion: Leidenfrost

We have investigated liquid helium Leidenfrost drops in the temperature range of 3.5-5.2 K, and we found that the ΔT of 1-70 mK needed to levitate the drops is much smaller than predicted by previous models, and much smaller than predicted by the onset of film boiling. We found that the Leidenfrost temperature T_L varies with the ambient temperature of the experimental cell, and that this temperature runs approximately parallel to the vapor pressure curve. We calculated vapor thickness if 700-1250 nm based on the properties and lifetime of the drop, and also the parameters of the experiment. We observe that the drops levitate just as easily over liquid as solid, and that the levitating drops transition freely between both a solid surface and a thin liquid pool.

References

[1] L. Maquet, B. Sobac, B. Darbois-Texier, A. Duchesne, M. Brandenbourger, A. Rednikov, P. Colinet, and S. Dorbolo, "Leidenfrost drops on a heated liquid pool," *Physical Review Fluids*, vol. 1, no. 5, p. 053902, 2016.

[2] A.-L. Biance, C. Clanet, and D. Quéré, "Leidenfrost drops," *Physics of Fluids*, vol. 15, no. 6, pp. 1632–1637, 2003.

[3] S. T. Thoroddsen and K. Takehara, "The coalescence cascade of a drop," *Physics of Fluids*, vol. 12, no. 6, pp. 1265–1267, 2000.

[4] C. Josserand and S. T. Thoroddsen, "Drop impact on a solid surface," *Annual review of fluid mechanics*, vol. 48, pp. 365–391, 2016.

[5] R. Rioboo, M. Marengo, and C. Tropea, "Time evolution of liquid drop impact onto solid, dry surfaces," *Exp. Fluids*, vol. 33, no. 1, pp. 112–124, 2002.

[6] P. Kavehpour, B. Ovryn, and G. H. McKinley, "Evaporatively-driven marangoni instabilities of volatile liquid films spreading on thermally conductive substrates," *Colloid Surf. A-Physicochem. Eng. Asp.*, vol. 206, no. 1-3, pp. 409–423, 2002.

[7] J. Lopez, C. A. Miller, and E. Ruckenstein, "Spreading kinetics of liquid-drops on solids," *J. Colloid Interface Sci.*, vol. 56, no. 3, pp. 460–468, 1976.

[8] A. L. Yarin and D. A. Weiss, "Impact of drops on solid-surfaces - self-similar capillary waves, and splashing as a new-type of kinematic discontinuity," *J. Fluid Mech.*, vol. 283, pp. 141–173, 1995.

[9] J. E. Sprittles and Y. D. Shikhmurzaev, "The dynamics of liquid drops and their interaction with solids of varying wettabilities," *Phys. Fluids*, vol. 24, no. 8, p. 17, 2012.

[10] C. Josserand and S. Zaleski, "Droplet splashing on a thin liquid film," *Phys. Fluids*, vol. 15, no. 6, pp. 1650–1657, 2003.

[11] A. B. Wang and C. C. Chen, "Splashing impact of a single drop onto very thin liquid films," *Phys. Fluids*, vol. 12, no. 9, pp. 2155–2158, 2000.

[12] A. B. Aljedaani, C. Wang, A. Jetly, and S. T. Thoroddsen, "Experiments on the breakup of drop-impact crowns by marangoni holes," *Journal of Fluid Mechanics*, vol. 844, pp. 162–186, 2018.

[13] D. F. Chao and N. L. Zhang, "Effects of evaporation and thermocapillary convection on volatile liquid droplets," *J. Thermophys. Heat Transf.*, vol. 15, no. 4, pp. 416–420, 2001.

[14] S. C. Case and S. R. Nagel, "Coalescence in low-viscosity liquids," *Phys. Rev. Lett.*, vol. 100, no. 8, p. 4, 2008.

[15] K. G. Winkels, J. H. Weijs, A. Eddi, and J. H. Snoeijer, "Initial spreading of low-viscosity drops on partially wetting surfaces," *Phys. Rev. E*, vol. 85, no. 5, p. 4, 2012.

[16] P. G. Degennes, "Wetting - statics and dynamics," *Rev. Mod. Phys.*, vol. 57, no. 3, pp. 827–863, 1985.

[17] A. M. Cazabat and M. A. C. Stuart, "Dynamics of wetting - effects of surface-roughness," *J. Phys. Chem.*, vol. 90, no. 22, pp. 5845–5849, 1986.

[18] D. Bonn, J. Eggers, J. Indekeu, J. Meunier, and E. Rolley, "Wetting and spreading," *Rev. Mod. Phys.*, vol. 81, no. 2, pp. 739–805, 2009.

[19] R. J. Donnelly, R. N. Hills, and P. H. Roberts, "Superflow in restricted geometries," *Phys. Rev. Lett.*, vol. 42, no. 11, pp. 725–728, 1979.

[20] J. F. Joanny, "Spreading of superfluid drops," *Journal De Physique*, vol. 46, no. 5, pp. 807–813, 1985.

[21] E. Cheng, M. W. Cole, J. Dupontroc, W. F. Saam, and J. Treiner, "Novel wetting behavior in quantum films," *Rev. Mod. Phys.*, vol. 65, no. 2, pp. 557–567, 1993.

[22] J. E. Rutledge and P. Taborek, "Prewetting phase-diagram of he-4 on cesium," *Phys. Rev. Lett.*, vol. 69, no. 6, pp. 937–940, 1992.

[23] D. Ross, J. E. Rutledge, and P. Taborek, "Superfluid droplets on a solid surface," *Science*, vol. 278, no. 5338, pp. 664–666, 1997.

[24] J. A. Phillips, P. Taborek, and J. E. Rutledge, "Experimental survey of wetting and superfluid onset of he-4 on alkali metal surfaces," *J. Low Temp. Phys.*, vol. 113, no. 5-6, pp. 829–834, 1998.

[25] H. Alles, A. V. Babkin, P. J. Hakonen, J. P. Ruutu, J. T. Salojarvi, and J. P. Saramaki, "Spreading of superfluid he-4 on mgf2," *J. Low Temp. Phys.*, vol. 102, no. 1-2, pp. 21–29, 1996.

[26] R. Luusalo, A. Husmann, J. Kopu, and P. Hakonen, "Pseudo-contact angles and pinned vorticity in superfluid he-4," *Physica B*, vol. 284, pp. 147–148, 2000.

[27] M. Poujade, C. Guthmann, and E. Rolley, "Apparent dewetting due to superfluid flow," *Europhys. Lett.*, vol. 58, no. 6, pp. 837–843, 2002.

[28] S. Herminghaus, "Can a superfluid droplet spread?" *Europhys. Lett.*, vol. 42, no. 4, pp. 443–448, 1998.

[29] N. B. Speirs, K. Langley, P. Taborek, and S. T. Thoroddsen, "Jet breakup in superfluid and normal liquid he 4," *Physical Review Fluids*, vol. 5, no. 4, p. 044001, 2020.

[30] J. Philippi, P.-Y. Lagrée, and A. Antkowiak, "Drop impact on a solid surface: short-time self-similarity," *Journal of Fluid Mechanics*, vol. 795, pp. 96–135, 2016.

[31] G. Riboux and J. M. Gordillo, "Experiments of drops impacting a smooth solid surface: a model of the critical impact speed for drop splashing," *Physical review letters*, vol. 113, no. 2, p. 024507, 2014.

[32] A. L. Biance, C. Clanet, and D. Quere, "First steps in the spreading of a liquid droplet," *Phys. Rev. E*, vol. 69, no. 1, p. 016301, 2004.

[33] A. Eddi, K. G. Winkels, and J. H. Snoeijer, "Short time dynamics of viscous drop spreading," *Phys. Fluids*, vol. 25, no. 1, p. 10, 2013.

[34] M. R. Davidson, "Spreading of an inviscid drop impacting on a liquid film," *Chem. Eng. Sci.*, vol. 57, no. 17, pp. 3639–3647, 2002.

[35] R. J. Donnelly and C. F. Barenghi, "The observed properties of liquid helium at the saturated vapor pressure," *J. Phys. Chem. Ref. Data*, vol. 27, no. 6, pp. 1217–1274, 1998.

[36] E. Aursand, "Film boiling and rapid phase transition of liquefied natural gas," 2019.

[37] M. Geri, B. Keshavarz, G. H. McKinley, and J. W. Bush, "Thermal delay of drop coalescence," *Journal of Fluid Mechanics*, vol. 833, 2017.

[38] R. Savino, D. Paterna, and M. Lappa, "Marangoni flotation of liquid droplets," *Journal of Fluid Mechanics*, vol. 479, pp. 307–326, 2003.

[39] P. Dell'Aversana and G. P. Neitzel, "When liquids stay dry." *Physics today*, vol. 51, no. 1, pp. 38–41, 1998.

[40] R. Monti, R. Savino, and S. Tempesta, "Wetting prevention by thermal marangoni effect. experimental and numerical simulation," *European Journal of Mechanics-B/Fluids*, vol. 17, no. 1, pp. 51–77, 1998.

[41] J. Leidenfrost, "De aquae communis nonnullis qualitatibus tractatus, 1756," *Int. J. Heat Mass Transfer*, vol. 9, no. 1153, 1966.

[42] P. Testa and L. Nicotra, "Influence of pressure on the leidenfrost temperature and on extracted heat fluxes in the transient mode and low pressure," *Journal of heat transfer*, vol. 108, no. 4, pp. 916–921, 1986.

[43] G. Emmerson and C. Snoek, "The effect of pressure on the leidenfrost point of discrete drops of water and freon on a brass surface," *International Journal of Heat and Mass Transfer*, vol. 21, no. 8, pp. 1081–1086, 1978.

[44] T. Roques-Carmes, A. Domps, P. Marchal, and L. Marchal-Heussler, "Equivalent capacitive thickness of the vapor layer below leidenfrost drops," *Experiments in Fluids*, vol. 59, no. 7, p. 115, 2018.

[45] M. A. Van Limbeek, M. H. K. Schaarsberg, B. Sobac, A. Rednikov, C. Sun, P. Colinet, and D. Lohse, "Leidenfrost drops cooling surfaces: theory and interferometric measurement," *Journal of fluid mechanics*, vol. 827, pp. 614–639, 2017.

[46] J. Burton, A. Sharpe, R. Van Der Veen, A. Franco, and S. Nagel, "Geometry of the vapor layer under a leidenfrost drop," *Physical review letters*, vol. 109, no. 7, p. 074301, 2012.

[47] J. M. Kolinski, S. M. Rubinstein, S. Mandre, M. P. Brenner, D. A. Weitz, and L. Mahadevan, "Skating on a film of air: drops impacting on a surface," *Physical review letters*, vol. 108, no. 7, p. 074503, 2012.

[48] S. Lyu, V. Mathai, Y. Wang, B. Sobac, P. Colinet, D. Lohse, and C. Sun, "Final fate of a leidenfrost droplet: Explosion or takeoff," *Science advances*, vol. 5, no. 5, p. eaav8081, 2019.

[49] F. Celestini, T. Frisch, and Y. Pomeau, "Take off of small leidenfrost droplets," *Physical review letters*, vol. 109, no. 3, p. 034501, 2012.

[50] N. Nagai and S. Nishio, "Leidenfrost temperature on an extremely smooth surface," *Experimental thermal and fluid science*, vol. 12, no. 3, pp. 373–379, 1996.

[51] D. Orejon, K. Sefiane, and Y. Takata, "Effect of ambient pressure on leidenfrost temperature," *Physical Review E*, vol. 90, no. 5, p. 053012, 2014.

[52] B. Sobac, A. Rednikov, S. Dorbolo, and P. Colinet, "Leidenfrost effect: Accurate drop shape modeling and refined scaling laws," *Physical Review E*, vol. 90, no. 5, p. 053011, 2014.

[53] J. Lienhard, "Correlation for the limiting liquid superheat," *Chemical Engineering Science*, vol. 31, no. 9, pp. 847–849, 1976.

[54] P. Spiegler, J. Hopenfeld, M. Silberberg, C. Bumpus Jr, and A. Norman, "Onset of stable film boiling and the foam limit," *International Journal of Heat and Mass Transfer*, vol. 6, no. 11, pp. 987–989, 1963.

[55] K. Baumeister and F. Simon, "Leidenfrost temperature—its correlation for liquid metals, cryogens, hydrocarbons, and water," *Journal of Heat Transfer*, vol. 95, no. 2, pp. 166–173, 1973.

[56] J. L. Miller, "Leidenfrost drops are on a roll," *Physics Today*, vol. 71, no. 11, pp. 14–15, 2018.

[57] M. Weilert, D. L. Whitaker, H. Maris, and G. Seidel, "Magnetic levitation of liquid helium," *Journal of low temperature physics*, vol. 106, no. 1-2, pp. 101–131, 1997.

[58] M. Shirota, M. A. van Limbeek, C. Sun, A. Prosperetti, and D. Lohse, "Dynamic leidenfrost effect: relevant time and length scales," *Physical review letters*, vol. 116, no. 6, p. 064501, 2016.

[59] S. Nukiyama, "The maximum and minimum values of the heat q transmitted from metal to boiling water under atmospheric pressure," *International Journal of Heat and Mass Transfer*, vol. 9, no. 12, pp. 1419–1433, 1966.

[60] J. S. Goodling and R. Irey, "Non-boiling and film boiling heat transfer to a saturated bath of liquid helium," in *Advances in cryogenic engineering*. Springer, 1969, pp. 159–169.

[61] W. Steward, "Transient helium heat transfer phase i—static coolant," *International Journal of Heat and Mass Transfer*, vol. 21, no. 7, pp. 863–874, 1978.

[62] T. R. Munro, J. P. Koeln, A. W. Fassmann, R. J. Barnett, and H. Ban, "Phase change heat transfer and bubble behavior observed on twisted wire heater geometries in microgravity," *International Journal of Heat and Fluid Flow*, vol. 47, pp. 21–30, 2014.

[63] T. R. Munro and H. Ban, "Flow and heat flux behavior of micro-bubble jet flows observed in thin, twisted-wire, subcooled boiling in microgravity," *Microgravity Science and Technology*, vol. 27, no. 1, pp. 49–60, 2015.